Hybrid User Pairing for Spectral and Energy Efficiencies in Multiuser MISO-NOMA Networks with SWIPT

Toan-Van Nguyen, *Student Member, IEEE,* Van-Dinh Nguyen, *Member, IEEE,* Daniel Benevides da Costa, *Senior Member, IEEE,* and Beongku An, *Member, IEEE*

***Abstract*—In this paper, we propose a novel hybrid user pairing (HUP) scheme in multiuser multiple-input single-output non-orthogonal multiple access networks with simultaneous wireless information and power transfer. In this system, two information users with distinct channel conditions are optimally paired while energy users perform energy harvesting (EH) under non-linearity of the EH circuits. We consider the problem of jointly optimizing user pairing and power allocation to maximize the overall spectral efficiency (SE) and energy efficiency (EE) subject to user-specific quality-of-service and harvested power requirements. A new paradigm for the EE-EH trade-off is then proposed to achieve a good balance of network power consumption. Such design problems are formulated as the maximization of non-concave functions subject to the class of mixed-integer non-convex constraints, which are very challenging to solve optimally. To address these challenges, we first relax binary pairing variables to be continuous and transform the design problems into equivalent non-convex ones, but with more tractable forms. We then develop low-complexity iterative algorithms to improve the objectives and converge to a local optimum by means of the inner approximation framework. Simulation results show the convergence of proposed algorithms and the SE and EE improvements of the proposed HUP scheme over state-of-the-art designs. In addition, the effects of key parameters such as the number of antennas and dynamic power at the BS, target data rates, and energy threshold, on the system performance are evaluated to show the effectiveness of the proposed schemes in balancing resource utilization.**

***Index Terms*—Energy efficiency, inner approximation, non-linear energy harvesting, non-orthogonal multiple access (NOMA), non-convex optimization, spectral efficiency, transmit beamforming, user pairing.**

The work of T. V. Nguyen and B. An was supported by the National Research Foundation of Korea (NRF) grant funded by the Korea government (MSIT) (No. 2019R1A2C1083996). The work of V.-D. Nguyen was supported in part by the Luxembourg National Research Fund (FNR) in the framework of the FNR-FNRS bilateral project "InWIP-NET: Integrated Wireless Information and Power Networks". The work of D. B. da Costa was supported by FUNCAP (Edital PRONEM, 01/2016) and by CNPq (Grant no. 302863/2017-6). Part of this paper has been presented in IEEE Global Communications Conference (GLOBECOM), Waikoloa, HI, USA, December 09-13, 2019.

T.-V. Nguyen is with the Dept. of Electronics and Computer Engineering in Graduate School, Hongik University, Republic of Korea (e-mail: vannguyen-toan@gmail.com).

V.-D. Nguyen is with the Interdisciplinary Centre for Security, Reliability and Trust (SnT) – University of Luxembourg, L-1855 Luxembourg (email: dinh.nguyen@uni.lu).

D. B. da Costa is with the Dept. of Computer Engineering, Federal University of Ceará, Sobral, CE, Brazil (e-mail: danielbcosta@ieee.org).

B. An is with Dept. of Software and Communications Engineering, Hongik University, Republic of Korea (e-mail: beongku@hongik.ac.kr).

I. Introduction

Recently, non-orthogonal multiple access (NOMA) has recognized as the promising multiple access technique for the evolving fifth generation (5G) of cellular networks since it provides high spectral efficiency (SE) and accommodates a large number of users [1], [2]. In power domain-based NOMA, a base station (BS) serves multiple users in the same time-frequency resources with different power allocation coefficients. Particularly, users with poor channel conditions get more power in order to improve their throughput, while successive interference cancellation (SIC) is applied for the users with better channel conditions to remove the interference from the former ones [3]. When users have similar channel conditions due to the same path loss, dynamic user clustering and user pairing are effective approaches to realize the viable benefits of NOMA in providing high SE and massive connectivity requirement of 5G networks [4]–[7].

Simultaneous wireless information and power transfer (SWIPT) has attracted significant attention due to its promising feature in extending lifetime of wireless networks [8], [9]. However, the increase of path loss attenuation during far-field wireless power transfer (WPT) is one of the most challenges faced by SWIPT systems [8]. To reduce such an attenuation, the optimization of the hardware architecture of energy harvesting (EH) circuits was a favorable approach to improve the energy conversion efficiency for wireless devices [9]. In practice, the input-output characteristic of EH circuits is highly non-linear, which leads to a mismatch for resource allocation and performance degradation [10]. To capture exactly behaviors of EH circuits in SWIPT systems, in this paper we consider a practical non-linear EH model and design energy beamforming (EB) at BS to maximize spectral efficiency and energy efficiency (EE).

In order to effectively reduce the system load while maintaining the quality-of-service (QoS) requirement of users in NOMA systems, hybrid NOMA has been considered by flexibly combining NOMA with orthogonal multiple-access (OMA). Particularly, users are first grouped in multiple pairs, in which NOMA is performed within each pair and different pairs are served by the conventional OMA to avoid inter-pair interference [7]. Recently, the optimal user pairing algorithm is capable of providing better SE performance than the random pairing in downlink NOMA systems [4], [11]. In [12], the authors proposed a user pairing scheme by adopting matching

theory to select users for pairing from preference list channel conditions. In multiuser (MU) multiple-input single-output (MISO) systems with SWIPT, the effects of multiuser interference and non-linear EH circuits, which were unpredictable and caused a mismatch for resource allocation, have received less attention. Thus, it is of crucial to unveil how the hybrid user pairing approach can improve the system performances from the perspective of SE and EE.

A. Related Works

Early literature on user pairing has considerably focused on maximizing spectral efficiency in NOMA downlink systems. For instance, in [11], various optimal user pairing-based scenarios were studied to improve SE performance considering minimal rate constraints for each user. In cellular networks, the user pairing process was handled by the BS with power allocation in a centralized management manner [7], [13]. Moreover, opportunistically pairing for users with distinct channel conditions greatly reduced the complexity of NOMA systems [13]. Based on the users' channel correlations, user grouping was applied in millimeter-Wave (mmWave) NOMA systems in [14] and mmWave massive multiple-input multiple-output (MIMO) NOMA systems with SWIPT in [15], where a joint design of user grouping, power allocation, analog and digital precoding approach showed the SE and EE improvements over its counterpart without user grouping. To further enhance the SE of MIMO-NOMA systems, [16] proposed user pairing and scheduling algorithms which not only pair the selected users but also schedule suitable pairs for data transmission. In addition to user pairing, user clustering and power allocation have recently been investigated in [17] to maximize SE in downlink MIMO-NOMA systems from the user fairness perspective.

Regarding MISO-NOMA SWIPT systems, the power splitting architecture was addressed in [18], where a user with better channel condition is acted as an EH relay for the poor channel condition one, with the goal of maximizing its data rate under serious feedback delay at the BS. Considering non-linear EH model, Zhang *et al.* in [19] formulated the transmission power and the total EH trade-off problem by using multi-objective optimization approach. To maximize the system secrecy throughput in MISO networks, a path following algorithm was proposed in [20] relying on the inner approximation (IA) framework to arrive at a suboptimal solution with the low complexity and rapid convergence. In [21], a joint design of beamforming and power splitting was considered in cooperative MISO-NOMA SWIPT systems to maximize the data rate of a strong user subject to the QoS requirement of a weak user.

However, the aforementioned works on MISO-NOMA SWIPT systems were mainly focused in maximizing average SE or enhancing the total EH. Only a few works have studied the effects of user pairing on energy efficiency, which is one of the key performance metrics in 5G. In [22], the weighted sum EE maximization problem with a new power consumption model was formulated in multi-cell downlink MISO systems, where such problem was latter efficiently solved by IA algorithms. A jointly designing SE-EE trade-off problem has also attracted much attention in recent literature, e.g., see [23]–[25]. In [23], a joint antenna selection and beamforming design was studied to achieve a good SE-EE trade-off region. It was proved in [24] that the system with an accurate channel estimator can achieve a good SE-EE trade-off. Under a similar target, a jointly optimizing transmit covariance matrices and transmit antenna selection was performed in MIMO systems [25], and power splitting in combination with beamforming problem was designed in [26] to maximize the achievable utility function (UF) in MISO-SWIPT systems considering both the system SE and total harvested power.

B. Motivation and Contributions

As mentioned above, the power allocation in combination with random user pairing in NOMA systems has been extensively researched. However, considering the hybrid user pairing together with energy beamforming design under the non-linearity of EH circuits in MISO-NOMA systems with SWIPT has not been properly studied in the literature. Motivated by the 5G network requirements and the benefits of MISO, NOMA and SWIPT, these concepts can be naturally linked together to realize an efficient type of network model with the SE and EE enhancements. In [27], the design of NOMA-enabled EH in MISO systems provided higher EE than the OMA one. An effective beamforming design in NOMA-enabled MISO-SWIPT systems also revealed its superior SE compared to the conventional OMA [28]. Beamforming design and cooperative transmission were studied in MISO-NOMA SWIPT systems in [29], [30] aiming to improve SE performance. By employing MISO, NOMA and SWIPT in 5G cellular Internet-of-Thing networks, the proposed system achieved its largest SE while consuming the lowest power under practical conditions of imperfect SIC, non-linear EH circuits and channel uncertainty [31]. Moreover, a general EE-EH trade-off problem for such systems has also remained comparatively open in the literature.

Different from recent works [3], [7], [11], we propose a novel hybrid user pairing beamforming (HUP) scheme for MU-MISO-NOMA downlink systems with SWIPT in order to maximize the achievable spectral and energy efficiencies. A more sophisticated EE-EH trade-off problem is also formulated to provide several meaningful insights into the network characterizations. In the proposed HUP scheme, two information users with distinct channel conditions are paired while energy users located nearby the BS perform energy harvesting. The implementation of hybrid user pairing method allows the BS to optimize information and energy beamformers, resulting in enhancement of the harvested power at energy users.

We consider a general MISO-NOMA system with SWIPT technique, where multiple information users and energy users are deployed randomly in a small cell area. Here, energy users with non-linear EH circuits can harvest energy and store in their local batteries for future use. In practice, all users are not required to group into clusters, however in this paper any two information users with distinct channel conditions will be grouped into clusters and perform NOMA. By adding user pairing approach, NOMA and SWIPT as design degrees to the optimization problem, the proposed hybrid user pairing is a

promising scheme to achieve better performance than state-of-the-art solutions, and on the other hand, makes the problems much more challenging than those considered in [32], [33] due to their high non-convex characteristics. Even if we split the formulated problem into subproblems (each subproblem with integer variables given by one of possible cases) to separately solve a simpler problem, the resulting subproblem is still non-convex with continuous variables. We leverage the IA framework [34] to develop an iterative algorithm that solves a second-order cone (SOC) program in each iteration, where the feasibility set in each step contains that of the previous one, and is always a subset of the feasibility set of the relaxed problem. The main contributions of the paper can be summarized as follows:

- We design the hybrid user pairing scheme by introducing new binary variables to optimally pair two information users with distinct channel conditions. The new design helps alleviate intra-pair interference and allows to exploit the full potential of NOMA for MISO-SWIPT networks.
- We formulate SE and EE optimization problems considering user pairing and non-linear EH circuit characteristics. These problems belong to the class of mixed-integer non-convex programming, which are very challenging to solve globally.
- Towards practical applications, we develop low-complexity iterative algorithms to solve the formulated problems. In particular, we first relax binary variables to be continuous and transform design problems into equivalent non-convex ones yet with more tractable forms. We note that the standard methods cannot be applied to solve these non-trivial problems directly. We then resort to the IA framework to tackle these non-convex relaxed problems. By novel approximations, problems obtained at each iteration can be cast as a SOC program for which modern convex solvers are very efficient. Simulation results latter reveal that pairing continuous variables found at optimum are close to exact binary values, arising as a near-optimal solution.
- We further formulate a more sophisticated EE-EH trade-off problem which captures the system EE and harvested power to design an accurate measurement on the network power consumption. The multi-objective optimization is proposed for such a problem that flexibly switches to the objective of maximizing EE or EH, depending on the target design of communication systems. As the extremely non-convex optimization problem, we develop an iterative algorithm based on the IA framework for its solution, where the approximate problem at each iteration is transformed into the SOC program for practical implementation.
- We show through numerical results the convergence of proposed algorithms, and the SE and EE improvements of the proposed HUP scheme over state-of-the-art designs, i.e., random user pairing (RUP) [5], and conventional multiuser beamforming (MUB) [35]. Moreover, the effects of key parameters such as the number of antennas and dynamic power at the BS, target data rates, and energy threshold, on the system performance are evaluated and discussed comprehensively.

The rest of the paper is arranged as follows. Section II introduces the system model and formulates the problems of SEM, EEM, and EE-EH trade-off. We devise the optimal solution for the SEM, EEM, and EE-EH trade-off problems in Section III, IV, and V, respectively. Section VI analyzes and discusses the convergence and complexity of the proposed algorithms. Numerical results are provided in Section VII, and Section VIII concludes the paper.

Notation: x, $\mathbf{x}$, and $\mathbf{X}$ denote a scalar, a vector, and a matrix, respectively. $[\mathbf{x}]_i$ denotes the i-th element of a vector $\mathbf{x}$ and $[\mathbf{X}]_{ij}$ represents the (i,j)-th element of a matrix. $\mathbb{C}$ and $\mathbb{R}$ are the sets of complex numbers and real numbers, respectively. $\|.\|$ and $|\cdot|$ indicate the L_2-norm and the absolute value, respectively. $\Re\{\cdot\}$ symbolizes the real part. $\mathcal{CN}(\boldsymbol{\eta}, \boldsymbol{Z})$ stands for circularly symmetric complex Gaussian (CSCG) distribution with mean $\boldsymbol{\eta}$ and covariance matrix $\boldsymbol{Z}$. Trace$(\cdot)$ designates the trace operator, and $\mathbb{E}\{\cdot\}$ denotes the expectation operator. $(\cdot)^T$, $(\cdot)^*$, and $(\cdot)^H$ are normal transpose, complex conjugate, and Hermitian transpose, respectively.

II. System Model and Problem Formulation

A. System Description

We consider a multiuser MISO downlink system, where a base station equipped with L antennas serves multiple single-antenna users in the same time-frequency resource, as depicted in Fig. 1. We assume that the BS is located at the center of network while users are uniformly distributed into two zones [5], [36]. Zone-1 is a smaller disc with inner radius r, while zone-2 is an annular area with outer radius R. There are a set $\mathcal{M} \triangleq \{\mathtt{ID}_m^{(1)}, m = 1, \ldots, M\}$ of M information users and a set $\mathcal{K} \triangleq \{\mathtt{EH}_k, k = 1, \ldots, K\}$ of K energy users in zone-1, and a set $\mathcal{N} \triangleq \{\mathtt{ID}_n^{(2)}, n = 1, \ldots, N\}$ of N information users in zone-2. It should be emphasized that information user $\mathtt{ID}_m^{(1)}$ in zone-1 has different channel condition compared to user $\mathtt{ID}_n^{(2)}$ in zone-2. Hence, $\mathtt{ID}_m^{(1)}$ is potentially grouped with $\mathtt{ID}_n^{(2)}$ to create a virtual pair[1] for NOMA transmission. Besides, the energy user $\mathtt{EH}_k$ can take the advantage of its proximity to the BS to harvest energy and store in its local battery for future use, e.g., processing the received signals or transmitting signals to the BS [26], [37]. We assume that all channels experience quasi-static independent identically distributed (i.i.d.) Rayleigh fading, and the channel state information (CSI) is available at both the BS and users [33], [36], [38]. In this system, we deploy the spatial transmit beamforming incorporated with NOMA to simultaneously serve multiple users at the same resource block (time, frequency, and spreading code). The BS transmits the information bearing signals to the information users using information beamforming while the power is simultaneously delivered to K energy users via energy beamforming matrix. Thus, the complex signals transmitted by the BS can be expressed as

[1]The pairing approach is able to reduce the BS load and signal processing delay while improving the performance of NOMA systems [36].

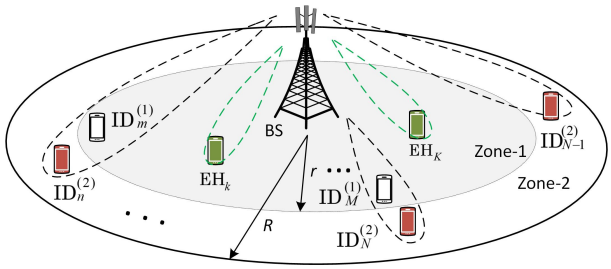

Fig. 1: Illustration of the downlink NOMA-assisted MISO-SWIPT system serving multiple information and energy users.

$$\mathbf{x} = \sum_{m\in\mathcal{M}} \mathbf{w}_m^{(1)} s_m + \sum_{n\in\mathcal{N}} \mathbf{w}_n^{(2)} s_n + \mathbf{v}_e, \tag{1}$$

where $\mathbf{w}_m^{(1)}$ and $\mathbf{w}_n^{(2)}$ denote the $L\times 1$ information beamforming vectors for $\mathtt{ID}_m^{(1)}$ and $\mathtt{ID}_n^{(2)}$, respectively; s_m with $\mathbb{E}\{|s_m|^2\}=1$ and s_n with $\mathbb{E}\{|s_n|^2\}=1$ are the signals intended for $\mathtt{ID}_m^{(1)}$ and $\mathtt{ID}_n^{(2)}$, respectively; $\mathbf{v}_e \sim \mathcal{CN}(\mathbf{0}, \mathbf{V}\mathbf{V}^H)$ represents the energy beam vector intended for K energy users with $\mathbf{V}\in\mathbb{C}^{L\times \bar{K}}$, where $\bar{K}\leq \min(L,K)$ is the concurrent energy streams. For notational convenience, we define $\mathbf{w}_1 \triangleq [\mathbf{w}_m^{(1)}]_{m\in\mathcal{M}}$, $\mathbf{w}_2 \triangleq [\mathbf{w}_n^{(2)}]_{n\in\mathcal{N}}$, and $\mathbf{w} \triangleq [\mathbf{w}_1^T\ \mathbf{w}_2^T]^T$. Considering a flat fading channel, the received signals at $\mathtt{ID}_m^{(1)}$, $\mathtt{ID}_n^{(2)}$, and $\mathtt{EH}_k$ can be expressed, respectively, as

$$\begin{aligned} y_m =& \mathbf{h}_m^H \mathbf{w}_m^{(1)} s_m + \sum_{m'\in\mathcal{M}\setminus\{m\}} \mathbf{h}_m^H \mathbf{w}_{m'}^{(1)} s_{m'} \\ &+ \sum_{n\in\mathcal{N}} \mathbf{h}_m^H \mathbf{w}_n^{(2)} s_n + \mathbf{h}_m^H \mathbf{v}_e + n_m, \end{aligned} \tag{2}$$

$$\begin{aligned} y_n =& \mathbf{h}_n^H \mathbf{w}_n^{(2)} s_n + \sum_{n'\in\mathcal{N}\setminus\{n\}} \mathbf{h}_n^H \mathbf{w}_{n'}^{(2)} s_{n'} \\ &+ \sum_{m\in\mathcal{M}} \mathbf{h}_n^H \mathbf{w}_m^{(1)} s_m + \mathbf{h}_n^H \mathbf{v}_e + n_n, \end{aligned} \tag{3}$$

$$y_k = \sum_{m\in\mathcal{M}} \mathbf{g}_k^H \mathbf{w}_m^{(1)} s_m + \sum_{n\in\mathcal{N}} \mathbf{g}_k^H \mathbf{w}_n^{(2)} s_n + \mathbf{g}_k^H \mathbf{v}_e + n_k, \tag{4}$$

where $\mathbf{h}_m$, $\mathbf{h}_n$, and $\mathbf{g}_k$ are the $L\times 1$ channel coefficient vectors from the BS to $\mathtt{ID}_m^{(1)}$, $\mathtt{ID}_n^{(2)}$, and $\mathtt{EH}_k$, respectively. The channel coefficient vector is modeled as $\mathbf{f} = \sqrt{\rho_f}\tilde{\mathbf{f}}$ with $\mathbf{f}\in\{\mathbf{h}_m, \mathbf{h}_n, \mathbf{g}_k\}$, where ρ_f is the large-scale fading and $\tilde{\mathbf{f}}$ is the small-scale fading vector whose entries are generated as independent CSCG random variables with distribution $\mathcal{CN}(0,1)$. From (4), the radio-frequency (RF) power at the input of EH circuits at $\mathtt{EH}_k$ is given by [9]

$$\mathtt{E}_k(\mathbf{w},\mathbf{V}) = \sum_{m\in\mathcal{M}} |\mathbf{g}_k^H \mathbf{w}_m^{(1)}|^2 + \sum_{n\in\mathcal{N}} |\mathbf{g}_k^H \mathbf{w}_n^{(2)}|^2 + \|\mathbf{g}_k^H \mathbf{V}\|^2. \tag{5}$$

To present exactly the non-linear end-to-end WPT characteristic at EH circuits, we consider a practical non-linear EH (NL-EH) model based on the logistic (sigmoid) function. The non-linear harvested power at $\mathtt{EH}_k$ is modeled as [9]

$$\mathtt{E}_k^{\mathtt{NL}}(\mathbf{w},\mathbf{V}) = \frac{\Delta_k}{1+\exp(-a_k(\mathtt{E}_k(\mathbf{w},\mathbf{V})-b_k))} - \Delta_k\Omega_k, \tag{6}$$

where $\Delta_k \triangleq \bar{P}_k^{\mathrm{DC}}/(1-\Omega_k)$, $\bar{P}_k^{\mathrm{DC}}$ denotes the maximum power harvested at $\mathtt{EH}_k$ when the EH circuit is saturated, a_k and b_k are the parameters of non-linear EH model capturing the joint effects of various non-linear phenomena caused by hardware limitations, and $\Omega_k = (1+\exp(a_k b_k))^{-1}$.

B. Proposed Hybrid User Pairing Beamforming Scheme

At the beginning of each time frame, BS performs user pairing for information users who are located in different zones with distinct channel conditions. Particularly, the user with good channel condition in zone-1, $\mathtt{ID}_m^{(1)}$, is opportunistically paired with the user with poor channel condition in zone-2, $\mathtt{ID}_n^{(2)}$. Once they are in pairs, NOMA principle will be applied in each pair, where the SIC is carried out at the user with good channel condition. More specifically, $\mathtt{ID}_m^{(1)}$ employs SIC to decode the $\mathtt{ID}_n^{(2)}$'s message, and then successively subtracts this message from the received signal to obtain its own information, while $\mathtt{ID}_n^{(2)}$ directly decodes its own message. In the event that $\mathtt{ID}_m^{(1)}$ and $\mathtt{ID}_n^{(2)}$ cannot be paired together, or when the number of users in zone-1 differs from that of zone-2 (i.e., $M\neq N$), the remaining users $|M-N|$ are not paired and will communicate directly with the BS through their own beamforming vectors without using NOMA. The use of two NOMA users in one cluster has been widely studied recently due to its simplicity for practical implementation [5], [11], [36]. The key benefit of this approach is low signal processing latency (possibly low hardware design) since the near user requires to decode and remove the signal of one far user only (or one iteration). It is noted that in the scheme of near user decoding and removing signals of all far users, it requires many iterations (corresponding the number of far users) to perform SIC, leading to high signal processing latency and residual SIC [33], [39]. In practice, NOMA may become inefficient if the channels of two paired users are not sufficiently distinct [7]. Thus, in the proposed HUP scheme, $\mathtt{ID}_m^{(1)}$ and $\mathtt{ID}_n^{(2)}$ are paired together if and only if the performance measure of interest is improved. To implement user pairing, we introduce a new matrix $\mathbf{A}\in\mathbb{R}^{M\times N}$ whose elements are expressed as

$$[\mathbf{A}]_{mn} = \begin{cases} 1, & \text{when } \mathtt{ID}_m \text{ pairs with } \mathtt{ID}_n, \\ 0, & \text{otherwise.} \end{cases} \tag{7}$$

The signal-to-interference-plus-noise ratio (SINR) at $\mathtt{ID}_m^{(1)}$ in decoding $\mathtt{ID}_n^{(2)}$'s message can be expressed as

$$\mathtt{SINR}_m^{s_n}(\mathbf{w},\mathbf{V}) = \frac{|\mathbf{h}_m^H \mathbf{w}_n^{(2)}|^2}{\Psi_{m,n}(\mathbf{w},\mathbf{V})}, \tag{8}$$

where $\Psi_{m,n}(\mathbf{w},\mathbf{V}) = \sum_{m\in\mathcal{M}} |\mathbf{h}_m^H \mathbf{w}_m^{(1)}|^2 + \sum_{n'\in\mathcal{N}\setminus\{n\}} |\mathbf{h}_m^H \mathbf{w}_{n'}^{(2)}|^2 + \|\mathbf{h}_m^H\mathbf{V}\|^2 + \sigma_m^2$.

In order to adjust the pairing process, the SINR at $\mathtt{ID}_m^{(1)}$ to decode its own signal involving the pairing element can be expressed as

$$\mathtt{SINR}_m^{\mathtt{HUP}}(\mathbf{w},\mathbf{V},\mathbf{A}) = \frac{|\mathbf{h}_m^H \mathbf{w}_m^{(1)}|^2}{\Xi_m(\mathbf{w},\mathbf{V},\mathbf{A})}, \tag{9}$$

where $\Xi_m(\mathbf{w},\mathbf{V},\mathbf{A}) = \sum_{m'\in\mathcal{M}\setminus\{m\}} |\mathbf{h}_m^H \mathbf{w}_{m'}^{(1)}|^2 + \|\mathbf{h}_m^H\mathbf{V}\|^2 + \sum_{n'\in\mathcal{N}} (1-[\mathbf{A}]_{mn'}) |\mathbf{h}_m^H \mathbf{w}_{n'}^{(2)}|^2 + \sigma_m^2$.

For $\mathtt{ID}_n^{(2)}$, it decodes directly its own message with the following SINR:

$$\mathtt{SINR}_n^{s_n}(\mathbf{w},\mathbf{V})=\frac{|\mathbf{h}_n^H\mathbf{w}_n^{(2)}|^2}{\Phi_n(\mathbf{w},\mathbf{V})}, \tag{10}$$

where $\Phi_n(\mathbf{w},\mathbf{V})=\sum\limits_{m\in\mathcal{M}}|\mathbf{h}_n^H\mathbf{w}_m^{(1)}|^2+\sum\limits_{n'\in\mathcal{N}\setminus\{n\}}|\mathbf{h}_n^H\mathbf{w}_{n'}^{(2)}|^2+\|\mathbf{h}_n^H\mathbf{V}\|^2+\sigma_n^2$.

Based on (8) and (10), the SINR for $\mathtt{ID}_n^{(2)}$ can be derived involving with the pairing element $[\mathbf{A}]_{mn}$ as

$$\mathtt{SINR}_n^{\mathtt{HUP}}(\mathbf{w},\mathbf{V},\mathbf{A})=\min_{m\in\mathcal{M}}\left\{\frac{|\mathbf{h}_n^H\mathbf{w}_n^{(2)}|^2}{\Phi_n(\mathbf{w},\mathbf{V})},\frac{|\mathbf{h}_m^H\mathbf{w}_n^{(2)}|^2}{[\mathbf{A}]_{mn}\Psi_{m,n}(\mathbf{w},\mathbf{V})}\right\}. \tag{11}$$

In (11), if $[\mathbf{A}]_{mn}=0$ (i.e., two users are not paired), the second term inside of the min operator will go to infinity. In other words, it implies that $\mathtt{ID}_n^{(2)}$ just decodes its own message only, i.e., $\mathtt{SINR}_n^{\mathtt{HUP}}(\mathbf{w},\mathbf{V},\mathbf{A})=\frac{|\mathbf{h}_n^H\mathbf{w}_n^{(2)}|^2}{\Phi_n(\mathbf{w},\mathbf{V})}$. Thus, the proposed HUP scheme is now switched to the conventional MUB scheme without using NOMA, which will be discussed in Remark 1.

Finally, the achievable rates in nat/sec/Hz for $\mathtt{ID}_m^{(1)}$ and $\mathtt{ID}_n^{(2)}$ can be expressed, respectively, as

$$\mathcal{R}_m^{\mathtt{HUP}}(\mathbf{w},\mathbf{V},\mathbf{A})=\ln(1+\mathtt{SINR}_m^{\mathtt{HUP}}(\mathbf{w},\mathbf{V},\mathbf{A})),\forall m\in\mathcal{M}, \tag{12}$$

$$\mathcal{R}_n^{\mathtt{HUP}}(\mathbf{w},\mathbf{V},\mathbf{A})=\ln(1+\mathtt{SINR}_n^{\mathtt{HUP}}(\mathbf{w},\mathbf{V},\mathbf{A})),\forall n\in\mathcal{N}. \tag{13}$$

Remark 1. *Considering SINRs of $\mathtt{ID}_m^{(1)}$ and $\mathtt{ID}_n^{(2)}$ defined by* (9) *and* (11)*, respectively, some interesting observations can be remarked as follows. When $[\mathbf{A}]_{mn}=1$, two users are paired randomly and the proposed HUP scheme is changed to the RUP one that was considered in [5]. When these users are not in a pair, i.e. $[\mathbf{A}]_{mn}=0$, the proposed HUP scheme is changed to the MUB one which also was studied in [26], [35]. Hence, the proposed HUP scheme is a general scenario and can be switched to RUP and MUB schemes by adjusting pairing element $[\mathbf{A}]_{mn}=1$ and $[\mathbf{A}]_{mn}=0$, respectively.*

C. Problem Formulation

1) SEM Problem Formulation: Our main goal is to maximize the spectral efficiency of the system under QoS constraints for each individual ID user, the power budget at the BS, EH constraints for EH users, and pairing constraints for ID users. Therefore, the network SEM problem can be mathematically formulated as

$$\mathtt{SEM}:\max_{\mathbf{w},\mathbf{V},\mathbf{A}}\mathcal{R}_{\sum}\triangleq\sum_{m\in\mathcal{M}}\mathcal{R}_m^{\mathtt{HUP}}(\mathbf{w},\mathbf{V},\mathbf{A})+\sum_{n\in\mathcal{N}}\mathcal{R}_n^{\mathtt{HUP}}(\mathbf{w},\mathbf{V},\mathbf{A}) \tag{14a}$$

$$\text{s. t. } \mathcal{R}_m^{\mathtt{HUP}}(\mathbf{w},\mathbf{V},\mathbf{A})\geq\bar{\mathsf{R}}_m,\quad\forall m\in\mathcal{M}, \tag{14b}$$

$$\mathcal{R}_n^{\mathtt{HUP}}(\mathbf{w},\mathbf{V},\mathbf{A})\geq\bar{\mathsf{R}}_n,\quad\forall n\in\mathcal{N}, \tag{14c}$$

$$\mathsf{E}_k^{\mathtt{NL}}(\mathbf{w},\mathbf{V})\geq\bar{\mathsf{E}}_k,\qquad\forall k\in\mathcal{K}, \tag{14d}$$

$$\|\mathbf{w}_1\|^2+\|\mathbf{w}_2\|^2+\|\mathbf{V}\|^2\leq P_{\mathrm{BS}}^{\max}, \tag{14e}$$

$$[\mathbf{A}]_{mn}\in\{0,1\},\forall m\in\mathcal{M},\forall n\in\mathcal{N}, \tag{14f}$$

$$\sum_{n\in\mathcal{N}}[\mathbf{A}]_{mn}\leq 1,\ \sum_{m\in\mathcal{M}}[\mathbf{A}]_{mn}\leq 1,\quad\forall m\in\mathcal{M},\forall n\in\mathcal{N}, \tag{14g}$$

where constraints (14b) and (14c) guarantee the QoS requirements for $\mathtt{ID}_m^{(1)}$ and $\mathtt{ID}_n^{(2)}$ with predefined thresholds $\bar{\mathsf{R}}_m\geq 0$ and $\bar{\mathsf{R}}_n\geq 0$, respectively. Constraint (14d) indicates that the minimum energy harvested by $\mathtt{EH}_k$ is larger than some target EH threshold $\bar{\mathsf{E}}_k$. Constraint (14e) presents the total power, which is upper bounded to the total power budget of the BS, $P_{\mathrm{BS}}^{\max}$. Constraints (14f) and (14g) present the criteria for ID users pairing. Finally, constraint (14g) ensures that each information user only pairs with one another.

2) EEM Problem Formulation: Another goal is to maximize the EE of the considered system setup, where the total hardware power consumption at BS and all users can be modeled as [32], [40]

$$\begin{aligned}P_{total}=&\frac{1}{\epsilon}(\|\mathbf{w}_1\|^2+\|\mathbf{w}_2\|^2+\|\mathbf{V}\|^2)+LP_{\mathtt{BS}}^{dyn}+P_{\mathtt{BS}}^{sta}\\&+\sum_{m\in\mathcal{M}}P_{\mathtt{ID}_m}^{sta}+\sum_{n\in\mathcal{N}}P_{\mathtt{ID}_n}^{sta}+\sum_{k\in\mathcal{K}}P_{\mathtt{EH}_k}^{sta},\end{aligned} \tag{15}$$

where $\epsilon\in(0,1]$ denotes the power amplifier efficiency of the BS, $P_{\mathtt{BS}}^{dyn}$ is the dynamic power consumption corresponding to the power radiation of all circuit blocks in each active radio-frequency chain, $P_{\mathtt{BS}}^{sta}$ is the static power consumed by the cooling system, power supply, etc. $P_{\mathtt{ID}_m}^{sta}$, $P_{\mathtt{ID}_n}^{sta}$, and $P_{\mathtt{EH}_k}^{sta}$ present the energy consumption of $\mathtt{ID}_m^{(1)}$, $\mathtt{ID}_n^{(2)}$, and $\mathtt{EH}_k$, respectively. By denoting $P_0\triangleq LP_{\mathtt{BS}}^{dyn}+P_{\mathtt{BS}}^{sta}+\sum_{m\in\mathcal{M}}P_{\mathtt{ID}_m}^{sta}+\sum_{n\in\mathcal{N}}P_{\mathtt{ID}_n}^{sta}+\sum_{k\in\mathcal{K}}P_{\mathtt{EH}_k}^{sta}$ as the total circuit power, the EEM problem is thus formulated as

$$\mathtt{EEM}:\max_{\mathbf{w},\mathbf{V},\mathbf{A}}\mathcal{E}_{\sum}\triangleq\frac{\sum\limits_{m\in\mathcal{M}}\mathcal{R}_m^{\mathtt{HUP}}(\mathbf{w},\mathbf{V},\mathbf{A})+\sum\limits_{n\in\mathcal{N}}\mathcal{R}_n^{\mathtt{HUP}}(\mathbf{w},\mathbf{V},\mathbf{A})}{\frac{1}{\epsilon}(\|\mathbf{w}_1\|^2+\|\mathbf{w}_2\|^2+\|\mathbf{V}\|^2)+P_0} \tag{16a}$$

$$\text{s. t. } (14b),(14c),(14d),(14e),(14f),(14g). \tag{16b}$$

It is clear that the objective function in (16) is non-convex with respect to $\mathbf{w}_1$, $\mathbf{w}_2$ and $\mathbf{V}$ which brings the difficulty in obtaining the optimal design for the EEM problem.

3) EE-EH Trade-Off Problem Formulation: In future wireless networks, the escalation of energy consumption directly results in the increase of greenhouse gas emission which negatively affects the environment and sustainable development worldwide. The energy in the communication systems should be used efficiently, and consequently there is the need of comprehensive energy consumption model for these systems. A promising performance metric which can optimally trade-off between the needs of improving system throughput and limiting energy consumption, while the amount of harvested energy is maximized under the non-linear EH circuit characteristics, is introduced as the energy efficiency-energy harvesting (EE-EH) trade-off problem. Furthermore, figuring out the EE-EH trade-off metric allows us to find practically achievable EE-EH regions and paves the way for designing a more accurate measurement on the power consumption in future wireless networks. Due to this, in this paper we address the EE-EH trade-off issue by designing a general EE-EH framework which can flexibly switch between EE and EH depending on the target design of communication systems.

To facilitate the EE-EH trade-off problem, we introduce a utility function that captures both energy efficiency and harvested power. Specifically, the UF is shown as a general definition of power consumption of the system considering not only the data rate but also the amount of harvested energy. Therefore, it would be more reasonable to propose a multi-objective optimization problem to obtain a good balance between energy efficiency and harvested power. The UF based on the multi-objective optimization approach can be expressed as [26], [41]

$$\mathcal{F}(\mathbf{w},\mathbf{V},\mathbf{A}) = \alpha \sum_{m\in\mathcal{M}} \frac{\mathcal{R}_m^{\texttt{HUP}}(\mathbf{w},\mathbf{V},\mathbf{A})}{\bar{\mathsf{R}}_m} + \alpha \sum_{n\in\mathcal{N}} \frac{\mathcal{R}_n^{\texttt{HUP}}(\mathbf{w},\mathbf{V},\mathbf{A})}{\bar{\mathsf{R}}_n} + (1-\alpha) \sum_{k\in\mathcal{K}} \frac{\mathsf{E}_k^{\texttt{NL}}(\mathbf{w},\mathbf{V})}{\bar{\mathsf{E}}_k}, \tag{17}$$

where $\alpha \in [0,1]$ denotes the weighting parameter to control the priority between EE and EH. $\bar{\mathsf{R}}_m$, $\bar{\mathsf{R}}_n$ and $\bar{\mathsf{E}}_k$ can be considered as reference parameters which make units of the two objective functions in (17) consistent and their numerical values are comparable [26]. The utility function $\mathcal{F}(\mathbf{w},\mathbf{V},\mathbf{A},\alpha)$ is modeled to exposure the system characteristic in using energy. Based on the power consumption model in (15), we jointly design the information and energy beamformers, and pairing condition for maximizing the efficiency of using power in the network. To this end, the EE-EH problem can be formulated as

$$\texttt{EE-EH}: \max_{\mathbf{w},\mathbf{V},\mathbf{A}} \mathcal{T}_{\texttt{EE-EH}} \triangleq \frac{\mathcal{F}(\mathbf{w},\mathbf{V},\mathbf{A})}{\frac{1}{\epsilon}(\|\mathbf{w}_1\|^2+\|\mathbf{w}_2\|^2+\|\mathbf{V}\|^2)+P_0} \tag{18a}$$

$$\text{s. t.} \quad (14b), (14c), (14d), (14e), (14f), (14g). \tag{18b}$$

Remark 2. *The EE-EH problem is generally multi-objective accounting for power consumption minimization, throughput maximization, and energy harvesting maximization [41]. The intuition behind the EE-EH trade-off optimization problem through the lens of network design is that the usage of energy is more flexible and efficient depending on the demand of network target by adjusting weight parameter. When the weighting parameter α is sufficient large in* (17)*, corresponding to the demand of maximizing energy efficiency, the EH becomes less significant and the EE-EH problem is changed into the EEM problem. When α is relatively small, corresponding to the demand of maximizing energy harvesting, the EE becomes less significant in* (17) *and the EE-EH problem aims at increasing the amount of harvested energy at mobile users.*

III. Proposed Algorithm for SEM Problem

It is highly challenging to find a globally optimal solution to (14) because of two reasons. First, due to the strong coupling between continuous variables $(\mathbf{w},\mathbf{V})$ and binary variables $\mathbf{A}$, an exhaustive search can be used to find an optimal solution to (14) with a very high computational complexity. Second, even when binary variables are fixed, problem (14) is still highly non-convex in continuous variables $(\mathbf{w},\mathbf{V})$. In practical networks, the computational complexity of using exhaustive search is exponentially growing when the number of users increases. This motivates us to design more practically fascinating approaches that can achieve a good solution with low complexity. In the following, we propose an iterative low-complexity algorithm to find a suboptimal solution, yet efficient to (14). To do so, we first transform (14) into an equivalent non-convex problem, but with a more tractable form, and then apply the IA framework to iteratively approximate the non-convex parts [34], [42].

A. Tractable Form of (14)

A standard way to overcome the binary nature of (14) is to relax binary variables to be continuous, i.e., constraint (14f) is re-expressed as $[\mathbf{A}]_{mn} \in [0,1]$. Thus, the relaxed problem of (14) is given as

$$\texttt{SEM-Relaxed}: \max_{\mathbf{w},\mathbf{V},\mathbf{A},\mathbf{r}} \bar{\mathcal{R}}_{\sum} \triangleq \sum_{m\in\mathcal{M}} \mathcal{R}_m^{\texttt{HUP}}(\mathbf{w},\mathbf{V},\mathbf{A}) + \sum_{n\in\mathcal{N}} \mathcal{R}_n^{\texttt{HUP}}(\mathbf{w},\mathbf{V},\mathbf{A}) \tag{19a}$$

$$\text{s. t.} \ [\mathbf{A}]_{mn} \in [0,1], \quad \forall m\in\mathcal{M}, n\in\mathcal{N}, \tag{19b}$$

$$(14b), (14c), (14d), (14e), (14g). \tag{19c}$$

We then introduce new variables $\mathbf{r} \triangleq \{r_m, r_n\}_{n\in\mathcal{N},m\in\mathcal{M}}$ and $\boldsymbol{\gamma} \triangleq \{\gamma_m,\gamma_n\}_{m\in\mathcal{M},n\in\mathcal{N}}$, where r_m and r_n, and γ_m and γ_n denote soft data rates and SINRs of $\texttt{ID}_m^{(1)}$ and $\texttt{ID}_n^{(2)}$, respectively, to rewrite (19) as

$$\max_{\mathbf{w},\mathbf{V},\mathbf{A},\mathbf{r},\boldsymbol{\gamma}} \ \bar{\mathcal{R}}_{\sum} \triangleq \sum_{m\in\mathcal{M}} r_m + \sum_{n\in\mathcal{N}} r_n \tag{20a}$$

$$\text{s. t.} \ \texttt{SINR}_m^{\texttt{HUP}}(\mathbf{w},\mathbf{V},\mathbf{A}) \geq 1/\gamma_m, \quad \forall m\in\mathcal{M}, \tag{20b}$$

$$\texttt{SINR}_n^{\texttt{HUP}}(\mathbf{w},\mathbf{V},\mathbf{A}) \geq 1/\gamma_n, \quad \forall n\in\mathcal{N}, \tag{20c}$$

$$\ln(1+1/\gamma_m) \geq r_m, \quad \forall m\in\mathcal{M}, \tag{20d}$$

$$\ln(1+1/\gamma_n) \geq r_n, \quad \forall n\in\mathcal{N}, \tag{20e}$$

$$r_m \geq \bar{\mathsf{R}}_m, \quad \forall m\in\mathcal{M}, \tag{20f}$$

$$r_n \geq \bar{\mathsf{R}}_n, \quad \forall n\in\mathcal{N}, \tag{20g}$$

$$(14d), (14e), (14g), (19b). \tag{20h}$$

We now provide the following proposition to characterize the relationship between problems (19) and (20).

Proposition 1. *Problems* (19) *and* (20) *are equivalent at optimum since they have the same optimal solution set $(\mathbf{w}^\star,\mathbf{V}^\star,\mathbf{A}^\star)$ and objective value $\bar{\mathcal{R}}_{\sum}^\star$.*

Proof: The equivalence between (19) and (20) is verified by showing that inequalities (20b)-(20e) must hold with equalities at optimum. The proof is detailed in Appendix A. ■

B. Proposed Iterative Algorithm

In problem (20), the objective (20a) is linear and concave function, and constraints (20b)−(20e), and (14d) are non-convex. Thus, we now pay a particular attention to handle non-convex parts of (20) following the IA principle.

Approximation of constraints (20b) *and* (20c)*:* First, constraint (20b) for $\mathtt{ID}_m^{(1)}$ user can be reformulated from (9) as

$$\frac{\Xi_m(\mathbf{w},\mathbf{V},\mathbf{A})}{\gamma_m} \le |\mathbf{h}_m^H\mathbf{w}_m^{(1)}|^2. \tag{21}$$

To arrive at a tractable form, we introduce additional variables $\boldsymbol{\tau} \triangleq \{\tau_{m,n} \ge 0\}_{m\in\mathcal{M},n\in\mathcal{N}}$ which satisfy the convex constraint $|\mathbf{h}_m^H\mathbf{w}_{n'}^{(2)}|^2 \le \tau_{m,n'}$, to rewrite (21) equivalently as

$$\begin{aligned}|\mathbf{h}_m^H\mathbf{w}_m^{(1)}|^2 \ge& \frac{1}{\gamma_m}\Big(\sum_{m'\in\mathcal{M}\setminus\{m\}}|\mathbf{h}_m^H\mathbf{w}_{m'}^{(1)}|^2 + \|\mathbf{h}_m^H\mathbf{V}\|^2+\sigma_m^2\\ &+\sum_{n'\in\mathcal{N}}(1-[\mathbf{A}]_{mn'})\tau_{m,n'}\Big) \triangleq \frac{1}{\gamma_m}\widehat{\Xi}_m(\mathbf{w},\mathbf{V},\mathbf{A},\boldsymbol{\tau}).\end{aligned} \tag{22}$$

The following lemmas are invoked to make (22) convex.

Lemma 1. *For any $x\in\mathbb{C}, y\in\mathbb{R}_{++}$, it is true that*

$$\frac{x^2}{y} \ge \frac{2\bar{x}^*}{\bar{y}}x - \frac{|\bar{x}|^2}{\bar{y}^2}y. \tag{23}$$

Proof: The proof of Lemma 1 is given Appendix A of [43]. ∎

Lemma 2. *For any $(x,y)\in\mathbb{R}_{++}^2$, it is true that*

$$\frac{1}{xy} \le \frac{1}{2}\Big(\frac{\bar{x}}{\bar{y}x^2}+\frac{\bar{y}}{\bar{x}y^2}\Big). \tag{24}$$

Proof: The proof of Lemma 2 is given [42]. It is noted that the right-hand side (RHS) of (24) is shown as a convex upper bound of function $1/(xy)$, making it become more refined in approximating the function $1/(xy)$ based on the IA framework. ∎

Let $x^{(\kappa)}$ indicate the feasible point of x at the κ-th iteration of an iterative algorithm. We are now in a position to make (22) convex, where the term $|\mathbf{h}_m^H\mathbf{w}_m^{(1)}|^2$ in the left-hand side (LHS) of (22) can be approximated by recalling Lemma 1 as

$$\begin{aligned}|\mathbf{h}_m^H\mathbf{w}_m^{(1)}|^2 &\ge 2\Re\big\{(\mathbf{h}_m^H\mathbf{w}_m^{(1),(\kappa)})^*(\mathbf{h}_m^H\mathbf{w}_m^{(1)})\big\} - |\mathbf{h}_m^H\mathbf{w}_m^{(1),(\kappa)}|^2\\ &\triangleq f_m^{(\kappa)}(\mathbf{w}_m^{(1)}),\end{aligned} \tag{25}$$

and $\widehat{\Xi}_m(\mathbf{w},\mathbf{V},\mathbf{A},\boldsymbol{\tau})$ can be iteratively upper bounded by invoking Lemma 2 as

$$\begin{aligned}&\widehat{\Xi}_m(\mathbf{w},\mathbf{V},\mathbf{A},\boldsymbol{\tau})\\ &\le \sum_{n'\in\mathcal{N}}\Big(\frac{1-[\mathbf{A}]_{mn'}^{(\kappa)}}{2\tau_{m,n'}^{(\kappa)}}\tau_{m,n'}^2 + \frac{\tau_{m,n'}^{(\kappa)}(1-[\mathbf{A}]_{mn'})^2}{2(1-[\mathbf{A}]_{mn'}^{(\kappa)})}\Big)\\ &\quad+\sum_{m'\in\mathcal{M}\setminus\{m\}}|\mathbf{h}_m^H\mathbf{w}_{m'}^{(1)}|^2+\|\mathbf{h}_m^H\mathbf{V}\|^2+\sigma_m^2\\ &\triangleq \widehat{\Xi}_m^{(\kappa)}(\mathbf{w},\mathbf{V},\mathbf{A},\boldsymbol{\tau}).\end{aligned} \tag{26}$$

Note that $\widehat{\Xi}_m^{(\kappa)}(\mathbf{w},\mathbf{V},\mathbf{A},\boldsymbol{\tau})$ is quadratic convex function and the global upper bound of $\widehat{\Xi}_m(\mathbf{w},\mathbf{V},\mathbf{A},\boldsymbol{\tau})$, satisfying $\widehat{\Xi}_m^{(\kappa)}(\mathbf{w}^{(\kappa)},\mathbf{V}^{(\kappa)},\mathbf{A}^{(\kappa)},\boldsymbol{\tau}^{(\kappa)}) = \widehat{\Xi}_m(\mathbf{w}^{(\kappa)},\mathbf{V}^{(\kappa)},\mathbf{A}^{(\kappa)},\boldsymbol{\tau}^{(\kappa)})$. Hence, (22) is iteratively replaced by the following convex constraint:

$$\frac{\widehat{\Xi}_m^{(\kappa)}(\mathbf{w},\mathbf{V},\mathbf{A},\boldsymbol{\tau})}{\gamma_m} \le f_m^{(\kappa)}(\mathbf{w}_m^{(1)}), \quad \forall m\in\mathcal{M}. \tag{27}$$

Turning our attention to constraint (20c) for user $\mathtt{ID}_n^{(2)}$ which can be rewritten as

$$\frac{1}{\gamma_n} \le \min_{m\in\mathcal{M}}\Big\{\frac{|\mathbf{h}_n^H\mathbf{w}_n^{(2)}|^2}{\Phi_n(\mathbf{w},\mathbf{V})}, \frac{|\mathbf{h}_m^H\mathbf{w}_n^{(2)}|^2}{[\mathbf{A}]_{mn}\Psi_{m,n}(\mathbf{w},\mathbf{V})}\Big\}. \tag{28}$$

Without loss of generality, inequality (28) can be replaced by

$$\begin{cases}\dfrac{1}{\gamma_n} \le \dfrac{|\mathbf{h}_n^H\mathbf{w}_n^{(2)}|^2}{[\Phi_n(\mathbf{w},\mathbf{V})]}, & \forall n\in\mathcal{N} \quad (29a)\\ \dfrac{1}{\gamma_n} \le \dfrac{|\mathbf{h}_m^H\mathbf{w}_n^{(2)}|^2}{\big([\mathbf{A}]_{mn}\Psi_{m,n}(\mathbf{w},\mathbf{V})\big)}, & \forall m\in\mathcal{M}, n\in\mathcal{N}. \quad (29b)\end{cases}$$

Inequality (29a) can be re-expressed as $\Phi_n(\mathbf{w},\mathbf{V})/\gamma_n \le |\mathbf{h}_n^H\mathbf{w}_n^{(2)}|^2$, where the term $|\mathbf{h}_n^H\mathbf{w}_n^{(2)}|^2$ can be lower bounded by invoking Lemma 1 as

$$\begin{aligned}|\mathbf{h}_n^H\mathbf{w}_n^{(2)}|^2 &\ge 2\Re\big\{(\mathbf{h}_n^H\mathbf{w}_n^{(2),(\kappa)})^*(\mathbf{h}_n^H\mathbf{w}_n^{(2)})\big\} - |\mathbf{h}_n^H\mathbf{w}_n^{(2),(\kappa)}|^2\\ &\triangleq f_n^{(\kappa)}(\mathbf{w}_n^{(2)}).\end{aligned} \tag{30}$$

Note that $\Phi_n(\mathbf{w},\mathbf{V})/\gamma_n$ is a quadratic-over-linear function, which is convex. Thus, (29a) can be approximated at iteration $\kappa+1$ as

$$\frac{\Phi_n(\mathbf{w},\mathbf{V})}{\gamma_n} \le f_n^{(\kappa)}(\mathbf{w}_n^{(2)}), \qquad \forall n\in\mathcal{N}. \tag{31}$$

Considering constraint (29b), it follows that

$$\frac{\Psi_{m,n}(\mathbf{w},\mathbf{V})}{\gamma_n} \le \frac{|\mathbf{h}_m^H\mathbf{w}_n^{(2)}|^2}{[\mathbf{A}]_{mn}}, \qquad \forall n\in\mathcal{N}, \tag{32}$$

where both sides are a quadratic-over-linear function. By recalling again Lemma 1, we address the RHS of (32) with its lower bound as

$$\begin{aligned}\frac{|\mathbf{h}_m^H\mathbf{w}_n^{(2)}|^2}{[\mathbf{A}]_{mn}} &\ge \frac{2\Re\big\{(\mathbf{h}_m^H\mathbf{w}_n^{(2),(\kappa)})^*(\mathbf{h}_m^H\mathbf{w}_n^{(2)})\big\}}{[\mathbf{A}]_{mn}^{(\kappa)}} - \frac{|\mathbf{h}_m^H\mathbf{w}_n^{(2),(\kappa)}|^2}{|[\mathbf{A}]_{mn}^{(\kappa)}|^2[\mathbf{A}]_{mn}^{-1}}\\ &\triangleq f_{m,n}^{(\kappa)}(\mathbf{w}_n^{(2)},[\mathbf{A}]_{mn}).\end{aligned} \tag{33}$$

Plugging (33) into (32), (29b) is iteratively replaced by the following convex constraint:

$$\frac{\Psi_{m,n}(\mathbf{w},\mathbf{V})}{\gamma_n} \le f_{m,n}^{(\kappa)}(\mathbf{w}_n^{(2)},[\mathbf{A}]_{mn}), \ \forall m\in\mathcal{M}, n\in\mathcal{N}. \tag{34}$$

Approximation of constraints (14d)*,* (20d) *and* (20e)*:* We tackle constraint (14d) by transforming it into the following equivalent form:

$$\mathtt{E}_k(\mathbf{w},\mathbf{V}) \ge b_k - \frac{1}{a_k}\ln\Big(\frac{\Delta_k}{\bar{\mathtt{E}}_k+\Delta_k\Omega_k}-1\Big) \triangleq \theta_k. \tag{35}$$

Note that the LHS of (35) is a convex function; thus, we apply Lemma 1 to innerly approximate it around the point $(\mathbf{w}^{(\kappa)},\mathbf{V}^{(\kappa)})$ as follows:

$$\begin{aligned}\mathtt{E}_k(\mathbf{w},\mathbf{V}) \ge& \sum_{m\in\mathcal{M}}\Big[2\Re\big\{(\mathbf{w}_m^{(1),(\kappa)})^H\mathbf{g}_k\mathbf{g}_k^H\mathbf{w}_m^{(1)}\big\} - |\mathbf{g}_k^H\mathbf{w}_m^{(1),(\kappa)}|^2\Big]\\ &+\sum_{n\in\mathcal{N}}\Big[2\Re\big\{(\mathbf{w}_n^{(2),(\kappa)})^H\mathbf{g}_k\mathbf{g}_k^H\mathbf{w}_n^{(2)}\big\} - |\mathbf{g}_k^H\mathbf{w}_n^{(2),(\kappa)}|^2\Big]\\ &+2\Re\big\{\mathrm{Trace}\big((\mathbf{V}^{(\kappa)})^H\mathbf{g}_k\mathbf{g}_k^H\mathbf{V}\big)\big\} - \|\mathbf{g}_k^H\mathbf{V}^{(\kappa)}\|^2\\ &\triangleq \mathtt{E}_k^{(\kappa)}(\mathbf{w},\mathbf{V}).\end{aligned} \tag{36}$$

Substituting (36) into (35), the inner convex approximation of (14d) is given as

$$\mathtt{E}_k^{(\kappa)}(\mathbf{w},\mathbf{V}) \geq \theta_k, \quad \forall k \in \mathcal{K}. \tag{37}$$

The LHSs of (20d) and (20e) are convex and logarithmic function, while their RHSs are linear. To solve these constraints more efficiently, we will approximate and convert them into SOC constraints. By applying the concave lower bound of the logarithmic function in [5, Eq. (66)], the function $\ln(1+\gamma^{-1})$ with $\gamma > 0$ can be approximated at iteration $\kappa+1$ as

$$\begin{aligned}\ln(1+\gamma^{-1}) \geq& \ln\left(1+(\gamma^{(\kappa)})^{-1}\right) + (\gamma^{(\kappa)}+1)^{-1} \\ &- \gamma\left[\gamma^{(\kappa)}(\gamma^{(\kappa)}+1)\right]^{-1} \triangleq \mathcal{A}^{(\kappa)}(\gamma),\end{aligned} \tag{38}$$

where $\gamma \in \{\gamma_m, \gamma_n\}_{m\in\mathcal{M},n\in\mathcal{N}}$.

From the above discussions, problem (20) can be approximated by the following convex program at iteration $\kappa+1$:

$$\max_{\substack{\mathbf{w},\mathbf{V},\mathbf{A},\\ \mathbf{r},\boldsymbol{\gamma},\boldsymbol{\tau}}} \bar{\mathcal{R}}_{\sum}^{(\kappa)} \triangleq \sum_{m\in\mathcal{M}} r_m + \sum_{n\in\mathcal{N}} r_n \tag{39a}$$

$$\text{s. t. } |\mathbf{h}_m^H \mathbf{w}_{n'}^{(2)}|^2 \leq \tau_{m,n'}, \quad \forall m \in \mathcal{M}, n' \in \mathcal{N}, \tag{39b}$$

$$\mathcal{A}^{(\kappa)}(\gamma_m) \geq r_m, \quad \forall m \in \mathcal{M}, \tag{39c}$$

$$\mathcal{A}^{(\kappa)}(\gamma_n) \geq r_n, \quad \forall n \in \mathcal{N}, \tag{39d}$$

$$(14e), (14g), (19b), (20f), (20g), (27), (31), (34), (37). \tag{39e}$$

After solving (39), we update the involved optimization variables for the next iteration until convergence. We have ascertained that an iterative algorithm for solving (39) will result in a solution containing many $[\mathbf{A}]_{mn}$ close to 0 and 1 but still inexact binary values. In other words, the optimal solution achieved by solving (39) is infeasible to the original problem (14). To overcome this issue, we introduce the rounding function after obtaining the optimal solution of problem (39) as

$$[\mathbf{A}]_{mn}^{\star} = \left\lfloor [\mathbf{A}]_{mn}^{(\kappa)} + 1/2 \right\rfloor, \quad \forall m \in \mathcal{M}, n \in \mathcal{N}. \tag{40}$$

In Algorithm 1, we summarize the proposed iterative algorithm to solve the SEM problem (14).

Generating Initial Feasible Point For SEM Problem: Since our approximations are based on IA framework, finding a feasible initial point for (20) is required for the IA-based algorithm in the first iterations to successfully initialize the computational procedure. However, it is challenging to find the feasible starting point of Algorithm 1 due to the complexity of the objective function and its constraints. One simple option is to generate random initial points until satisfying constraints (20b)−(20h). However, this method is very inefficient or even fails to initialize the computational procedure. It is therefore nontrivial to develop a simple yet efficient way to find a feasible initial point so that Algorithm 1 is successfully solved in the first iterations. To do so, we provide an initialization method which makes QoS constraints feasible (i.e., (14d), (20f), and (20g)). Based on the development presented before and by any initial point $(\mathbf{w}^{(0)}, \mathbf{V}^{(0)}, \mathbf{A}^{(0)}, \boldsymbol{\gamma}^{(0)}, \boldsymbol{\tau}^{(0)})$, we

Algorithm 1 Proposed Iterative Algorithm for Solving SEM Problem (14)

1: **Initialization:** Set $\kappa \coloneqq 0$, $(\mathbf{w}^\star, \mathbf{V}^\star, \mathbf{A}^\star) \coloneqq 0$, and generate an initial feasible point $(\mathbf{w}^{(0)}, \mathbf{V}^{(0)}, \mathbf{A}^{(0)}, \boldsymbol{\gamma}^{(0)}, \boldsymbol{\tau}^{(0)})$ for (20) by solving (41).
2: **repeat**
3: Solve the convex program (39) to obtain the optimal solution $(\mathbf{w}^\star, \mathbf{V}^\star, \mathbf{A}^\star, \boldsymbol{\gamma}^\star, \boldsymbol{\tau}^\star)$;
4: Update $(\mathbf{w}^{(\kappa+1)}, \mathbf{V}^{(\kappa+1)}, \mathbf{A}^{(\kappa+1)}, \boldsymbol{\gamma}^{(\kappa+1)}, \boldsymbol{\tau}^{(\kappa+1)}) \coloneqq (\mathbf{w}^\star, \mathbf{V}^\star, \mathbf{A}^\star, \boldsymbol{\gamma}^\star, \boldsymbol{\tau}^\star)$;
5: Set $\kappa \coloneqq \kappa + 1$;
6: **until** Convergence
7: Update $(\mathbf{w}^\star, \mathbf{V}^\star) \coloneqq (\mathbf{w}^{(\kappa)}, \mathbf{V}^{(\kappa)})$ and $\mathbf{A}^\star$ as (40);
8: Calculate $\mathcal{R}_{\sum}$ in (14a) based on $(\mathbf{w}^\star, \mathbf{V}^\star, \mathbf{A}^\star)$;
9: **Output:** $\mathcal{R}_{\sum}$ and the optimal solution $(\mathbf{w}^\star, \mathbf{V}^\star, \mathbf{A}^\star)$.

successively solve the following convex program:

$$\max_{\substack{\mathbf{w},\mathbf{V},\\ \mathbf{A},\mathbf{r},\boldsymbol{\gamma}}} \delta_{\mathtt{SEM}} \triangleq \min_{\substack{m\in\mathcal{M},\\ n\in\mathcal{N},k\in\mathcal{K}}} \left\{ r_m - \bar{\mathsf{R}}_m, r_n - \bar{\mathsf{R}}_n, \mathtt{E}_k^{(\kappa)}(\mathbf{w},\mathbf{V}) - \theta_k \right\} \tag{41a}$$

$$\text{s. t. } (14e), (14g), (19b), (27), (31), (34), (39b), (39c), (39d), \tag{41b}$$

until achieving $\delta_{\mathtt{SEM}} \geq 0$, which outputs a feasible initial point for Algorithm 1.

IV. Proposed Algorithm For EEM Problem

In general, solving the EEM problem (16) is even more challenging than the SEM problem (14), since the former is a mixed-integer non-convex fractional programming which requires exponential complexity to find its optimal solution. However, we will show in the sequel that the IA framework applied for the SEM problem can be well extended to the EEM problem.

Similarly to (19), the relaxed problem of (16) is given as

$$\mathtt{EEM-Relaxed}: \max_{\mathbf{w},\mathbf{V},\mathbf{A}} \bar{\mathcal{E}}_{\sum} \triangleq \frac{\sum_{m\in\mathcal{M}} \mathcal{R}_m^{\mathtt{HUP}}(\mathbf{w},\mathbf{V},\mathbf{A}) + \sum_{n\in\mathcal{N}} \mathcal{R}_n^{\mathtt{HUP}}(\mathbf{w},\mathbf{V},\mathbf{A})}{\frac{1}{\epsilon}(\|\mathbf{w}_1\|^2 + \|\mathbf{w}_2\|^2 + \|\mathbf{V}\|^2) + P_0} \tag{42a}$$

$$\text{s. t. } [\mathbf{A}]_{mn} \in [0,1], \quad \forall m \in \mathcal{M}, n \in \mathcal{N}, \tag{42b}$$

$$(14b), (14c), (14d), (14e), (14g). \tag{42c}$$

We first introduce a new variable $t > 0$ which satisfies the constraint

$$\epsilon^{-1}(\|\mathbf{w}_1\|^2 + \|\mathbf{w}_2\|^2 + \|\mathbf{V}\|^2) + P_0 \leq t, \tag{43}$$

to rewrite the relaxed EEM problem (42) equivalently as

$$\max_{\mathbf{w},\mathbf{V},\boldsymbol{\alpha},t} \bar{\mathcal{E}}_{\sum} \triangleq \sum_{m\in\mathcal{M}} \frac{\mathcal{R}_m^{\mathtt{HUP}}(\mathbf{w},\mathbf{V},\mathbf{A})}{t} + \sum_{n\in\mathcal{N}} \frac{\mathcal{R}_n^{\mathtt{HUP}}(\mathbf{w},\mathbf{V},\mathbf{A})}{t} \tag{44a}$$

$$\text{s. t. } (14b), (14c), (14d), (14e), (14g), (42b), (43). \tag{44b}$$

The equivalence between (42) and (44) can be easily verified by the fact that constraint (43) must hold with equality at

optimum. Although problem (44) is highly non-convex, it can be transformed to the convex program by adopting the same IA framework as the SEM problem (20). By reusing the variables introduced in (20), problem (44) can be equivalently expressed as

$$\max_{\mathbf{w},\mathbf{V},\mathbf{A},\mathbf{e},\boldsymbol{\gamma},t} \ \bar{\mathcal{E}}_{\sum} \triangleq \sum_{m\in\mathcal{M}} e_m + \sum_{n\in\mathcal{N}} e_n \tag{45a}$$

$$\text{s. t.} \ \ \mathtt{SINR}_m(\mathbf{w},\mathbf{V},\mathbf{A}) \geq 1/\gamma_m, \quad \forall m\in\mathcal{M}, \tag{45b}$$

$$\mathtt{SINR}_n(\mathbf{w},\mathbf{V},\mathbf{A}) \geq 1/\gamma_n, \quad \forall n\in\mathcal{N}, \tag{45c}$$

$$\ln(1+1/\gamma_m)/t \geq e_m, \quad \forall m\in\mathcal{M}, \tag{45d}$$

$$\ln(1+1/\gamma_n)/t \geq e_n, \quad \forall n\in\mathcal{N}, \tag{45e}$$

$$\ln(1+1/\gamma_m) \geq \bar{\mathsf{R}}_m, \quad \forall m\in\mathcal{M}, \tag{45f}$$

$$\ln(1+1/\gamma_n) \geq \bar{\mathsf{R}}_n, \quad \forall n\in\mathcal{N}, \tag{45g}$$

$$(14d), (14e), (14g), (42b), (43), \tag{45h}$$

where $\mathbf{e} \triangleq \{e_m, e_n\}_{m\in\mathcal{M},n\in\mathcal{N}}$ are new variables. In problem (45), non-convex parts include (45b)-(45g) and (14d) which are already addressed in Section III, except for (45d) and (45e). The function $\ln(1+1/\gamma)/t$ with $\gamma \in \{\gamma_m, \gamma_n\}$ is convex in (γ, t), which can be approximated at a feasible point $(\gamma^{(\kappa)}, t^{(\kappa)})$ as [44, Eq. (18)]:

$$\begin{aligned}\frac{\ln(1+1/\gamma)}{t} &\geq \frac{2\ln(1+1/\gamma^{(\kappa)})}{t^{(\kappa)}} + \frac{1}{t^{(\kappa)}(\gamma^{(\kappa)}+1)} \\ &\quad - \frac{\gamma}{t^{(\kappa)}\gamma^{(\kappa)}(\gamma^{(\kappa)}+1)} - \frac{\ln(1+1/\gamma^{(\kappa)})}{(t^{(\kappa)})^2}t, \\ &\triangleq \mathcal{B}^{(\kappa)}(\gamma,t), \qquad \forall t^{(\kappa)}>0, \gamma^{(\kappa)}>0.\end{aligned} \tag{46}$$

In summary, at the $(\kappa+1)$-th iteration we solve the following convex program:

$$\max_{\substack{\mathbf{w},\mathbf{V},\mathbf{A},\\ \mathbf{e},\boldsymbol{\gamma},\boldsymbol{\tau},t}} \bar{\mathcal{E}}_{\sum} \triangleq \sum_{m\in\mathcal{M}} e_m + \sum_{n\in\mathcal{N}} e_n \tag{47a}$$

$$\text{s. t.} \ \ \mathcal{B}^{(\kappa)}(\gamma_m,t) \geq e_m, \quad \forall m\in\mathcal{M}, \tag{47b}$$

$$\mathcal{B}^{(\kappa)}(\gamma_n,t) \geq e_n, \quad \forall n\in\mathcal{N}, \tag{47c}$$

$$\mathcal{A}^{(\kappa)}(\gamma_m) \geq \bar{\mathsf{R}}_m, \quad \forall m\in\mathcal{M}, \tag{47d}$$

$$\mathcal{A}^{(\kappa)}(\gamma_n) \geq \bar{\mathsf{R}}_n, \quad \forall n\in\mathcal{N}, \tag{47e}$$

$$(14e), (14g), (27), (31), (34), (37), (39b), (42b), (43), \tag{47f}$$

where $\mathcal{A}^{(\kappa)}(\gamma)$ was defined in (38).

We outline the proposed iterative algorithm for solving the EEM problem (16) in Algorithm 2. *Generating Initial Feasible Point For EEM Problem:* To generate the initial feasible point for the EEM problem, we apply the similar initialization approach of the SEM problem by successively solving the following convex optimization problem:

$$\max_{\substack{\mathbf{w},\mathbf{V},\mathbf{A},\\ \mathbf{e},\boldsymbol{\gamma},\boldsymbol{\tau},t}} \delta_{\mathtt{EEM}} \triangleq \min_{\substack{m\in\mathcal{M},\\ n\in\mathcal{N},k\in\mathcal{K}}} \Big\{\mathcal{A}^{(\kappa)}(\gamma_m) - \bar{\mathsf{R}}_m, \mathcal{A}^{(\kappa)}(\gamma_n) - \bar{\mathsf{R}}_n, \mathsf{E}_k^{(\kappa)}(\mathbf{w},\mathbf{V}) - \theta_k\Big\} \tag{48a}$$

$$\text{s. t.} \ \ (14e), (14g), (27), (31), (34), (39b), (42b), (43), (47b), (47c), \tag{48b}$$

Algorithm 2 Proposed Iterative Algorithm for Solving EEM Problem (16)

1: **Initialization:** Set $\kappa := 0, (\mathbf{w}^\star, \mathbf{V}^\star, \mathbf{A}^\star) := 0$, and generate an initial feasible point $(\mathbf{w}^{(0)}, \mathbf{V}^{(0)}, \mathbf{A}^{(0)}, \boldsymbol{\gamma}^{(0)}, \boldsymbol{\tau}^{(0)}, t^{(0)})$ for (45) by solving (48).
2: **repeat**
3: Solve the convex program (47) to obtain the optimal solution $(\mathbf{w}^\star, \mathbf{V}^\star, \mathbf{A}^\star, \boldsymbol{\gamma}^\star, \boldsymbol{\tau}^\star, t^\star)$;
4: Update $(\mathbf{w}^{(\kappa+1)}, \mathbf{V}^{(\kappa+1)}, \mathbf{A}^{(\kappa+1)}, \boldsymbol{\gamma}^{(\kappa+1)}, \boldsymbol{\tau}^{(\kappa+1)}, t^{(\kappa+1)}) := (\mathbf{w}^\star, \mathbf{V}^\star, \mathbf{A}^\star, \boldsymbol{\gamma}^\star, \boldsymbol{\tau}^\star, t^\star)$;
5: Set $\kappa := \kappa + 1$;
6: **until** Convergence
7: Update $(\mathbf{w}^\star, \mathbf{V}^\star) := (\mathbf{w}^{(\kappa)}, \mathbf{V}^{(\kappa)})$ and $\mathbf{A}^\star$ as (40);
8: Calculate $\mathcal{E}_{\sum}$ in (16a) based on $(\mathbf{w}^\star, \mathbf{V}^\star, \mathbf{A}^\star)$;
9: **Output:** $\mathcal{E}_{\sum}$ and the optimal solution $(\mathbf{w}^\star, \mathbf{V}^\star, \mathbf{A}^\star)$.

until reaching $\delta_{\mathtt{EEM}} \geq 0$.

V. Proposed Algorithm for EE-EH Trade-off Problem

In this section, the EE-EH trade-off is provided to show the resource allocation problem for the usage of power in the network. Specifically, the EE-EH problem trade-off is equivalent to the multi-objective optimization problem of balancing the EE and EH maximization. From (18), the EE-EH problem can be rewritten as

$$\mathtt{EE{\cdot}EH}: \max_{\mathbf{w},\mathbf{V},\mathbf{A}} \mathcal{T}_{\mathtt{EE{\cdot}EH}} \triangleq \frac{\sum_{m\in\mathcal{M}} \zeta_m \mathcal{R}_m^{\mathtt{HUP}}(\mathbf{w},\mathbf{V},\mathbf{A}) + \sum_{n\in\mathcal{N}} \zeta_n \mathcal{R}_n^{\mathtt{HUP}}(\mathbf{w},\mathbf{V},\mathbf{A}) + \sum_{k\in\mathcal{K}} \zeta_k \mathsf{E}_k^{\mathtt{NL}}(\mathbf{w},\mathbf{V})}{\frac{1}{\epsilon}(\|\mathbf{w}_1\|^2 + \|\mathbf{w}_2\|^2 + \|\mathbf{V}\|^2) + P_0} \tag{49a}$$

$$\text{s. t.} \ \ (14b), (14c), (14d), (14e), (14f), (14g), \tag{49b}$$

where $\zeta_m \triangleq \alpha/\bar{\mathsf{R}}_m$, $\zeta_n \triangleq \alpha/\bar{\mathsf{R}}_n$, and $\zeta_k = (1-\alpha)/\bar{\mathsf{E}}_k$. The relaxed problem of (49) is

$$\mathtt{EE{\cdot}EH{-}Relaxed}: \max_{\mathbf{w},\mathbf{V},\mathbf{A}} \bar{\mathcal{T}}_{\mathtt{EE{\cdot}EH}} \triangleq \frac{\sum_{m\in\mathcal{M}} \zeta_m \mathcal{R}_m^{\mathtt{HUP}}(\mathbf{w},\mathbf{V},\mathbf{A}) + \sum_{n\in\mathcal{N}} \zeta_n \mathcal{R}_n^{\mathtt{HUP}}(\mathbf{w},\mathbf{V},\mathbf{A}) + \sum_{k\in\mathcal{K}} \zeta_k \mathsf{E}_k^{\mathtt{NL}}(\mathbf{w},\mathbf{V})}{\frac{1}{\epsilon}(\|\mathbf{w}_1\|^2 + \|\mathbf{w}_2\|^2 + \|\mathbf{V}\|^2) + P_0} \tag{50a}$$

$$\text{s. t.} \ \ [\mathbf{A}]_{mn} \in [0,1], \quad \forall m\in\mathcal{M}, n\in\mathcal{N}, \tag{50b}$$

$$(14b), (14c), (14d), (14e), (14g). \tag{50c}$$

In the same manner with (45), we can further equivalently rewrite problem (50) as

$$\max_{\substack{\mathbf{w},\mathbf{V},\mathbf{A},\\ \mathbf{e},\boldsymbol{\gamma},t}} \sum_{m\in\mathcal{M}} \zeta_m e_m + \sum_{n\in\mathcal{N}} \zeta_n e_n + \sum_{k\in\mathcal{K}} \zeta_k \frac{\mathsf{E}_k^{\mathtt{NL}}(\mathbf{w},\mathbf{V})}{t} \tag{51a}$$

$$\text{s. t.} \ \ (14d), (14e), (14g), (43), (45b)-(45g), (50b). \tag{51b}$$

Given the developments in Section IV, only the non-concave function $\sum_{k\in\mathcal{K}} \zeta_k \frac{\mathsf{E}_k^{\mathtt{NL}}(\mathbf{w},\mathbf{V})}{t}$ in (51a) needs to be tackled. By introducing new variables $\mathbf{z} \triangleq \{z_k\}_{k\in\mathcal{K}}$, $\sum_{k\in\mathcal{K}} \zeta_k \frac{\mathsf{E}_k^{\mathtt{NL}}(\mathbf{w},\mathbf{V})}{t}$ can

be equivalently expressed as

$$\sum_{k\in\mathcal{K}} \zeta_k \Delta_k \frac{z_k}{t}, \tag{52}$$

which imposes the constraint

$$\left[1+\exp(-a_k(\mathtt{E}_k(\mathbf{w},\mathbf{V})-b_k))\right]^{-1} - \Omega_k \geq z_k. \tag{53}$$

By Lemma 1, the concave lower bound of $\frac{z_k}{t}$ in (52) is given as

$$\frac{z_k}{t} \geq \frac{2\sqrt{z_k^{(\kappa)} z_k}}{t^{(\kappa)}} - \frac{z_k^{(\kappa)}}{(t^{(\kappa)})^2} t \triangleq \beta^{(\kappa)}(z_k, t). \tag{54}$$

For constraint (53), it follows that

$$(53) \Leftrightarrow \begin{cases} (1+u_k)^{-1} - \Omega_k \geq z_k, \forall k \in \mathcal{K}, & \text{(55a)} \\ \exp(-a_k(\mathtt{E}_k(\mathbf{w},\mathbf{V})-b_k)) \leq u_k, \forall k \in \mathcal{K}, & \text{(55b)} \end{cases}$$

where $\mathbf{u} \triangleq \{u_k\}_{k\in\mathcal{K}}$ are new variables. Constraint (55a) can be further rewritten as

$$1 - \Omega_k - \Omega_k u_k - z_k \geq u_k z_k. \tag{56}$$

We note that the function $u_k z_k$ is jointly concave with respect to u_k and z_k on the domain $u_k > 0, z_k > 0$, and its convex upper bound can be found by recalling Lemma 2 as

$$u_k z_k \leq \frac{1}{2}\left(\frac{u_k^{(\kappa)}}{z_k^{(\kappa)}} z_k^2 + \frac{z_k^{(\kappa)}}{u_k^{(\kappa)}} u_k^2\right) \triangleq \chi^{(\kappa)}(z_k, u_k). \tag{57}$$

For constraint (55b), we have

$$\mathtt{E}_k(\mathbf{w},\mathbf{V}) + {a_k}^{-1}\ln(u_k) \geq b_k. \tag{58}$$

It is noted that the function $\mathtt{E}_k(\mathbf{w},\mathbf{V})$ is convex and its lower bound approximation can be obtained by using the same approach in (36). The function $\ln(u_k)$ is a concave on the domain $u_k > 0$, and its lower bound inner approximation can be found by applying [5, Eq. (32)] as

$$\ln(u_k) \geq \ln(u_k^{(\kappa)}) + 1 - \frac{u_k^{(\kappa)}}{u_k} \triangleq \phi^{(\kappa)}(u_k). \tag{59}$$

As a result, constraint (55) is iteratively replaced by the following convex ones:

$$\begin{cases} 1 - \Omega_k - \Omega_k u_k - z_k \geq \chi^{(\kappa)}(z_k, u_k), & \text{(60a)} \\ \mathtt{E}_k^{(\kappa)}(\mathbf{w},\mathbf{V}) + {a_k}^{-1}\phi^{(\kappa)}(u_k) \geq b_k. & \text{(60b)} \end{cases}$$

Based on the discussion above and the approximations in (47), we solve the following convex program at the $(\kappa+1)$-th iteration:

$$\max_{\substack{\mathbf{w},\mathbf{V},\mathbf{A},\mathbf{e},\\ \boldsymbol{\gamma},\boldsymbol{\tau},\mathbf{z},\mathbf{u},t}} \bar{\mathcal{T}}_{\mathtt{EE\cdot EH}}^{(\kappa)} \triangleq \sum_{m\in\mathcal{M}} \zeta_m e_m + \sum_{n\in\mathcal{N}} \zeta_n e_n + \sum_{k\in\mathcal{K}} \zeta_k \Delta_k \beta^{(\kappa)}(z_k, t) \tag{61a}$$

$$\text{s. t.} \quad \text{(14e)}, \text{(14g)}, \text{(27)}, \text{(31)}, \text{(34)}, \text{(37)}, \text{(39b)}, \text{(43)}, \text{(47b)}, \text{(47c)}, \text{(47d)}, \text{(47e)}, \text{(50b)}, \text{(60)}. \tag{61b}$$

In Algorithm 3, we describe the proposed IA-based algorithm for solving the EE-EH problem (18).

Algorithm 3 Proposed Iterative Algorithm for Solving EE-EH Problem (18)

1: **Initialization:** Set $\kappa := 0$, $(\mathbf{w}^\star, \mathbf{V}^\star, \mathbf{A}^\star) := 0$, and generate an initial feasible point $(\mathbf{w}^{(0)}, \mathbf{V}^{(0)}, \mathbf{A}^{(0)}, \boldsymbol{\gamma}^{(0)}, \boldsymbol{\tau}^{(0)}, \mathbf{z}^{(0)}, \mathbf{u}^{(0)}, t^{(0)},)$ for (51) by solving (62).
2: **repeat**
3: Solve the convex program (61) to obtain the optimal solution $(\mathbf{w}^\star, \mathbf{V}^\star, \mathbf{A}^\star, \boldsymbol{\gamma}^\star, \boldsymbol{\tau}^\star, \mathbf{z}^\star, \mathbf{u}^\star, t^\star)$;
4: Update $(\mathbf{w}^{(\kappa+1)}, \mathbf{V}^{(\kappa+1)}, \mathbf{A}^{(\kappa+1)}, \boldsymbol{\gamma}^{(\kappa+1)}, \boldsymbol{\tau}^{(\kappa+1)}, \mathbf{z}^{(\kappa+1)}, \mathbf{u}^{(\kappa+1)}, t^{(\kappa+1)}) := (\mathbf{w}^\star, \mathbf{V}^\star, \mathbf{A}^\star, \boldsymbol{\gamma}^\star, \boldsymbol{\tau}^\star, \mathbf{z}^\star, \mathbf{u}^\star, t^\star)$;
5: Set $\kappa := \kappa + 1$;
6: **until** Convergence
7: Update $(\mathbf{w}^\star, \mathbf{V}^\star) := (\mathbf{w}^{(\kappa)}, \mathbf{V}^{(\kappa)})$ and $\mathbf{A}^\star$ as (40).
8: Calculate $\mathcal{T}_{\mathtt{EE\cdot EH}}$ in (18a) based on $(\mathbf{w}^\star, \mathbf{V}^\star, \mathbf{A}^\star)$.
9: **Output:** $\mathcal{T}_{\mathtt{EE\cdot EH}}$ and the optimal solution $(\mathbf{w}^\star, \mathbf{V}^\star, \mathbf{A}^\star)$.

Generating Initial Feasible Point For EE-EH Problem: To initialize the iterative procedure of Algorithm 3, we successively solve the following simpler convex program of (61):

$$\max_{\substack{\mathbf{w},\mathbf{V},\mathbf{A},\mathbf{e},\\ \boldsymbol{\gamma},\boldsymbol{\tau},\mathbf{z},\mathbf{u},t}} \delta_{\mathtt{EE\cdot EH}} \triangleq \min_{\substack{m\in\mathcal{M},\\ n\in\mathcal{N},k\in\mathcal{K}}} \Big\{ \mathcal{A}^{(\kappa)}(\gamma_m) - \bar{\mathsf{R}}_m, \mathcal{A}^{(\kappa)}(\gamma_n) - \bar{\mathsf{R}}_n, \mathtt{E}_k^{(\kappa)}(\mathbf{w},\mathbf{V}) - \theta_k \Big\} \tag{62a}$$

$$\text{s. t.} \quad \text{(14e)}, \text{(14g)}, \text{(27)}, \text{(31)}, \text{(34)}, \text{(39b)}, \text{(43)}, \text{(47b)}, \text{(47c)}, \text{(50b)}, \text{(60)}, \tag{62b}$$

until reaching $\delta_{\mathtt{EE\cdot EH}} \geq 0$.

VI. Convergence and Complexity Analysis

A. Convergence Analysis

In this subsection, we theoretically provide the convergence analysis of the proposed algorithms. We recall that Algorithms 1, 2 and 3 are developed to solve the relaxed problems (19), (42) and (50), respectively. For compact representation, we define the sets of optimization variables and updated variables of Algorithms 1, 2 and 3 as

$$\mathbf{S}_{\mathtt{SEM}} \triangleq \{\mathbf{w}, \mathbf{V}, \mathbf{A}, \boldsymbol{\gamma}, \boldsymbol{\tau}\}, \text{ and}$$
$$\mathbf{S}_{\mathtt{SEM}}^{(\kappa)} \triangleq \{\mathbf{w}^{(\kappa)}, \mathbf{V}^{(\kappa)}, \mathbf{A}^{(\kappa)}, \boldsymbol{\gamma}^{(\kappa)}, \boldsymbol{\tau}^{(\kappa)}\},$$
$$\mathbf{S}_{\mathtt{EEM}} \triangleq \{\mathbf{w}, \mathbf{V}, \mathbf{A}, \boldsymbol{\gamma}, \boldsymbol{\tau}, t\}, \text{ and}$$
$$\mathbf{S}_{\mathtt{EEM}}^{(\kappa)} \triangleq \{\mathbf{w}^{(\kappa)}, \mathbf{V}^{(\kappa)}, \mathbf{A}^{(\kappa)}, \boldsymbol{\gamma}^{(\kappa)}, \boldsymbol{\tau}^{(\kappa)}, t^{(\kappa)}\},$$
$$\mathbf{S}_{\mathtt{EE\cdot EH}} \triangleq \{\mathbf{w}, \mathbf{V}, \mathbf{A}, \boldsymbol{\gamma}, \boldsymbol{\tau}, t, \mathbf{z}, \mathbf{u}\}, \text{ and}$$
$$\mathbf{S}_{\mathtt{EE\cdot EH}}^{(\kappa)} \triangleq \{\mathbf{w}^{(\kappa)}, \mathbf{V}^{(\kappa)}, \mathbf{A}^{(\kappa)}, \boldsymbol{\gamma}^{(\kappa)}, \boldsymbol{\tau}^{(\kappa)}, t^{(\kappa)}, \mathbf{z}^{(\kappa)}, \mathbf{u}^{(\kappa)}\},$$

respectively. The convergence results of Algorithms 1, 2 and 3 for solving the relaxed problems are stated in the following proposition.

Proposition 2. *Algorithms 1, 2 and 3 produce the sequences* $\{\mathbf{S}_{\mathtt{SEM}}^{(\kappa)}\}$, $\{\mathbf{S}_{\mathtt{EEM}}^{(\kappa)}\}$ *and* $\{\mathbf{S}_{\mathtt{EE\cdot EH}}^{(\kappa)}\}$ *of improved solutions of* (20), (45) *and* (51) *(hence,* (19), (42) *and* (50)*), respectively, which converge to a Karush–Kuhn–Tucker (KKT) point.*

Proof: The convergence of IA-based algorithms can be found in [34]. To be self-contained, we provide the proof of Proposition 2 in Appendix B. ■

Remark 3. *From Proposition 2, the obtained solutions of Algorithms 1, 2 and 3 for solving the relaxed problems converge at least to local optima which satisfy the KKT conditions. The performance loss of the proposed algorithms compared to the optimal solution is mainly attributed to the use of the rounding function in* (40)*. However, we have numerically observed that the solution of the relaxed binary variables at optimum is very close to 0 or 1, resulting in a very slightly sub-optimal solution. The gap between the proposed algorithms and the optimal one (i.e., brute-force search) will be elaborated in Section VII.*

B. Complexity Analysis

We now provide the worst-case per-iteration complexity analysis of Algorithms 1, 2 and 3. It is clear that the complexity of the proposed algorithms is mainly contributed by solving the convex programs (i.e., Step 3). The convex optimization programs (39), (47) and (61) only involve SOC and linear constraints, leading to a low computational complexity. For the sake of notational simplicity, we denote by n_c and m_c with $c \in \{1, 2, 3\}$ the numbers of scalar optimization variables and linear/SOC constraints, respectively. The worst-case per-iteration computational complexity of Algorithms 1, 2 and 3 is provided in Table I.

VII. Numerical Results

In this section, we present illustrative numerical results for the achievable performance of the proposed algorithms. Following [5], [36], [45], we consider the small cell downlink network topology with $K = 5$ energy users, $M = 3$ information users in zone-1, $N = 4$ information users in zone-2, the number of antennas at BS $L = 7$. The large-scale fading is modeled as $\rho_f \triangleq 10^{-\sigma_{\rm PL}/10}$, where $\sigma_{\rm PL}$ presents the path loss (in dB). Without loss of generality, we set the target rate threshold of all information users to $\bar{\mathsf{R}} = \bar{\mathsf{R}}_m = \bar{\mathsf{R}}_n$. The obtained SE results in nats/sec/Hz are divided by $\ln(2)$ to achieve the corresponding results in bits/sec/Hz. Unless stated otherwise, the general simulation parameters used in this paper are taken from [5], [26], and shown in Table II. The convex solver SDPT3 [46] and the toolbox YALMIP [47] are used in the MATLAB environment to solve the convex program, where the iterative procedure of each algorithm is terminated when the increase in objective function between two consecutive iterations is less than 10^{-5}. The simulation result in each figure is obtained by averaging over 1000 independent channel realizations.

To emphasize the effectiveness of the proposed pairing approach, we compare the performance of HUP scheme with that of RUP and MUB schemes. The solutions for SEM, EEM and EE-EH problems of MUB scheme can be obtained by setting all the elements of matrix $\mathbf{A}$ in (39), (47), and (61), respectively, to be zero. In RUP scheme, if two users are randomly paired, the corresponding element of matrix $\mathbf{A}$ will be set to one, so that the new pairing matrix is obtained. Then, by replacing the matrix $\mathbf{A}$ in (39), (47), and (61) with the new pairing matrix in the previous step, we obtain the solutions of the RUP scheme for SEM, EEM and EE-EH problems, respectively. With these arrangements, the RUP and MUB schemes can be simulated from the problem of HUP scheme. Moreover, we provide the simulation results of the optimal scheme, i.e., brute-force search (BFS) algorithm, to find the best user-pairing scheme among $\max(M, N)!/(|N - M|)!$ possibilities. The complexity of each subproblem in the BFS algorithm can be calculated in the same way with Algorithm 1 but without binary variables. The numbers of scalar optimization variables and linear/SOC constraints in the BFS algorithm are $n_B = (L+3)(M+N)+L\bar{K}$ and $m_B = 2MN+3(M+N)+K+1$, respectively. Therefore, the total complexity of BFS algorithm is $\max(M, N)!/(|N - M|)! \times \mathcal{O}(n_B^2 m_B^{2.5} + m_B^{3.5})$, which is very high computational complexity even for networks of medium size. Therefore, it is utilized typically for benchmarking purposes.

Fig. 2 illustrates the typical convergence behavior of Algorithms 1, 2 and 3 for a given set of channel realizations which are generated randomly for three cases with $P_{\rm BS}^{\max} = 35$ dBm. Each point on the curve of Figs. 2(a), 2(b), and 2(c) is plotted by solving problems (39), (47), and (61), respectively. As can be observed, three algorithms converge to their optimal values within 10 iterations because they can search for an improved solution over the whole feasible set in each iteration. It also reveals the effectiveness of our approaches in terms of generating the initial points for Algorithms 1, 2 and 3 in (41), (48), and (62), respectively, which reduces the number of iterations required for convergence.

We study the average spectral efficiency of the considered schemes against the power budget, $P_{\rm BS}^{\max}$, as shown in Fig. 3(a). In this figure, results obtained by BFS algorithm are labeled as "BFS scheme". As can be observed, average SEs of all schemes are linearly increased with respect to $P_{\rm BS}^{\max}$ because the BS with high power budget can provide better services to ID users. As expected, the BFS scheme provides the highest SE because of finding the best user-pairing scheme among all possibilities. The gap between the BFS scheme and the proposed HUP one is mainly due to the introduction of the rounding function in (40) (after obtaining the optimal solution to recover exact binary values). The loss of performance of the proposed HUP scheme over the BFS one is illustrated in Fig. 3(a), which is also quantified in Table III. It can be seen that the gap is relatively small and narrower when the BS's transmit power increases. However, the BFS scheme requires extremely high complexity since the number of subproblems scales exponentially with the number of users, and thus, it only serves as a benchmark scheme. Statistically, the SE of the proposed HUP scheme only deviates around 2% from the optimal SE which reveals the excellent performance with much less complexity than the BFS scheme. It is not surprising that the proposed HUP scheme outperforms the RUP and MUB ones in all regions of $P_{\rm BS}^{\max}$. The reason is that the HUP scheme optimally selects two suitable users with distinct channels for pairing to achieve the largest possible SE while the RUP scheme selects randomly any two users for pairing

TABLE I: THE PER-ITERATION COMPLEXITY ANALYSIS OF THE PROPOSED ALGORITHMS

Alg.	n_c	m_c	Per-iteration complexity
Alg. 1	$(L+3)(M+N)+MN+L\bar{K}$	$3MN+4(M+N)+K+1$	$\mathcal{O}(n_1^2 m_1^{2.5}+m_1^{3.5})$
Alg. 2	$(L+3)(M+N)+MN+L\bar{K}+1$	$3MN+4(M+N)+K+2$	$\mathcal{O}(n_2^2 m_2^{2.5}+m_2^{3.5})$
Alg. 3	$(L+3)(M+N)+MN+L\bar{K}+2K+1$	$3MN+4(M+N)+3K+2$	$\mathcal{O}(n_3^2 m_3^{2.5}+m_3^{3.5})$

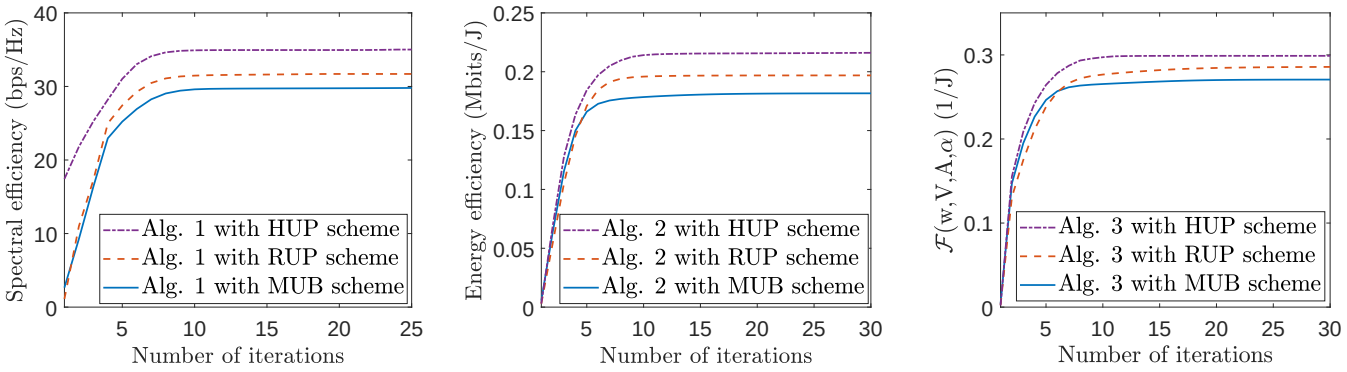

(a) Convergence of Algorithm 1 for SEM problem (b) Convergence of Algorithm 2 for EEM problem (c) Convergence of Algorithm 3 for EE-EH trade-off problem

Fig. 2: Convergence of Algorithms 1, 2, and 3 with HUP, RUP and MUB schemes.

TABLE II: SIMULATION PARAMETERS

Parameters	Value
Bandwidth	20 (MHz)
Noise power spectral density, $\sigma_m^2 = \sigma_n^2$	-174 (dBm/Hz)
Power consumption at BS, P_{BS}^{dyn} and P_{BS}^{sta}	10 and 15 (dBm)
Power consumption at users, $P_{\text{ID}_m}^{sta} = P_{\text{ID}_n}^{sta} = P_{\text{EH}_k}^{sta}$	5 (dBm)
Path loss at distance d (km), σ_{PL}	$140.7+37.6\log_{10}(d)$ (dB)
Radius of the cell, R	500 (m)
Coverage of the inner zone, r	200 (m)
Distance from BS to nearest user	$\geq$ 10 (m)
Power budge at the BS, $P_{\text{BS}}^{\max}$	35 (dBm)
Target rate threshold, $\bar{\text{R}}$	1 (bps/Hz)
Target energy harvesting threshold, $\bar{\text{E}}_k$	-55 (dBm)
Parameters for non-linear EH model, M_k and (a_k, b_k), $\forall k \in \mathcal{K}$	24 mW and $(150, 0.0014)$ [10].

TABLE III: THE AVERAGE SE OF THE BFS AND HUP SCHEMES

P_{BS} (dBm)	30	35	40	45	50
BFS scheme (bits/s/Hz)	20.3573	30.4024	38.6645	47.7109	56.0820
HUP scheme (bits/s/Hz)	18.6994	28.6573	37.3895	46.5310	55.6715

and it is apparently provided lower performance. Moreover, there is no user pairing in MUB scheme resulting in the worst performer. To further demonstrate the effectiveness of designing energy beamformer on the SE performance, we plot the average SE of the HUP scheme without energy beamforming, i.e., $\mathbf{V} = 0$, which is labeled as "HUP w/o EB". As can be seen, the proposed HUP scheme greatly outperforms its counterpart without EB because the BS has to sacrifice a part of its energy to power EH users as well as satisfy constraint (14d). This leads to the poor average SE of HUP w/o EB scheme, especially at the low value of the power budget $P_{\text{BS}}^{\max}$.

Fig. 3(b) reveals the average SE of the considered schemes as a function of the minimum rate requirement of each ID user. As can be observed, the highest average SE is achieved by the HUP scheme while its counterpart without energy beamforming is the lowest performer. As mentioned earlier, the BS in HUP w/o EB scheme has to sacrifice its energy to transfer enough power to EH users while the QoS of ID users is still guaranteed. This easily depletes the BS's energy when the user's QoS requirement is high, leading to the lowest system SE performance. In MUB scheme, the BS also allocates much power budget to serve separately users in different zones; thus, the average SE is degraded when the ID user's QoS requirement is increased. Differently, in RUP scheme, an ID user can mitigate the interference from the other one when they are in a pair, thus providing higher system SE. However, randomly selecting two users for pairing is not a favorable method when they have similar channel conditions. The proposed HUP scheme solves this drawback by selecting optimally two users with distinct channel conditions for pairing, thus it obtains quickly the satisfactory solution of ID user pairing and EH users constraints. This allows the system to maintain its QoS requirement even under the high data rate regime.

Fig. 3(c) plots the average SE against the number of antennas equipped at the BS, L. As can be observed, the average SE of all scheme is significantly increased when L is large. These results can be explained by considering the fact that the more degrees of freedom (DoF) are contributed to the system when the number of antennas is increased, the more efficient resource is utilized. Again, the proposed HUP

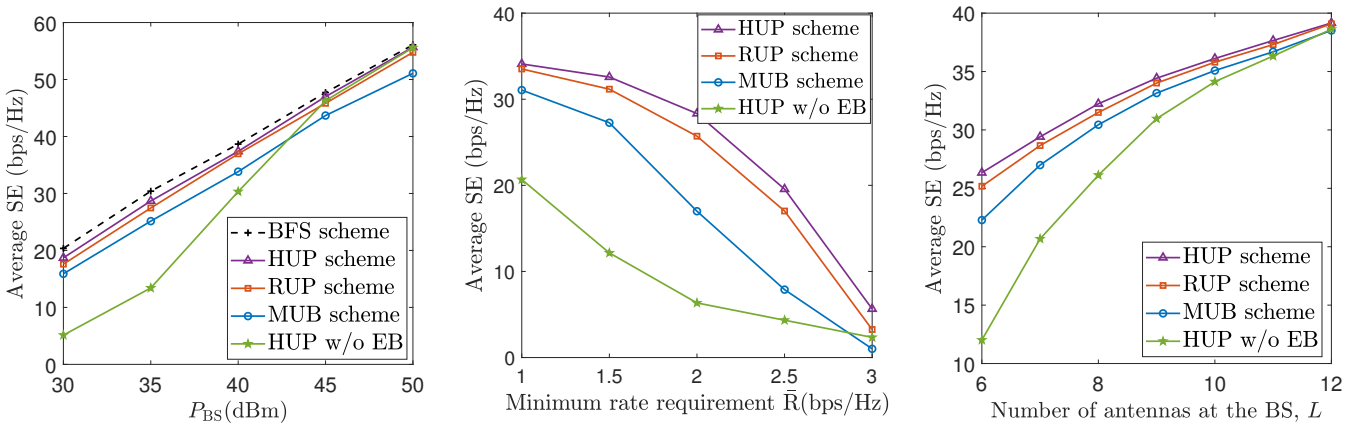

(a) Average SE versus $P_{\rm BS}^{\max}$ (b) Average SE versus $\bar{\rm R}$ (c) Average SE versus L

Fig. 3: Average SE versus $P_{\rm BS}^{\max}$, $\bar{\rm R}$, and L with EH threshold $\bar{\rm E}_k = -55$ dBm.

scheme enjoys a considerable improvement of the average SE as compared to the RUP, MUB and HUP w/e EB schemes. For small L, i.e., $L \leq 8$, the performance gap between HUP and MUB schemes is large due to the lack of DoF, arising the importance of using NOMA transmission in the considered network. When the number of antennas is larger than the total number of information users, i.e., $L > 7$, the effect of interference-free conditions becomes less significant in MUB scheme. Thus, the SE of MUB scheme is increased asymptotically to the RUP and HUP ones. A small number of antennas equipped at the BS result in the energy depletion for the HUP w/e EB scheme, and thus it again witnesses the lowest SE performance.

Fig. 4(a) sketches the cumulative distribution function (CDF) of the considered schemes as a function of the average SE with $\bar{\rm E}_k = -55$ dBm. It can be seen that the probabilities of feasibility of all schemes are smaller when the average SE is increased. In particular, the HUP scheme achieves the highest performance among the considered schemes, confirming the advantage of the proposed hybrid user pairing method and energy beamforming design. Besides, the HUP w/o EB scheme has a high probability that its achievable SE is less than 22 dBm, showing that it is an unstable design for the MISO-NOMA SWIPT systems. Finally, the HUP scheme reaches 1 Mbits/s and 2.2 Mbits/s of SE higher than the RUP and MUB schemes, respectively, in about 85% of simulated trials.

Fig. 4(b) shows the average SE versus target EH threshold $\bar{\rm E}_k$ in a setup with $P_{\rm BS}^{\max} = 35$ dBm and $\bar{\rm R} = 1$ (bps/Hz). As can be observed, the average SE-target EH threshold regions of all scheme are narrowed when $\bar{\rm E}_k$ is increased. Particularly, the SE of HUP w/o EB scheme starts to decrease dramatically at the small value of energy threshold, i.e., $\bar{\rm E}_k = -60$ dBm, while other schemes begin to diminish at $\bar{\rm E}_k = -45$ dBm. Specifically, the SE of all schemes is infeasible when $\bar{\rm E}_k$ is larger than -32 dBm, which also reveals a high influence of energy threshold on the system SE. For a small $\bar{\rm E}_k$, the small portion of received signal can fulfill the harvested power requirement, and thus the BS mainly allocates its power for ID users. However, when the $\bar{\rm E}_k$ becomes large, more power needs to be allocated to EH users to make the (14d) feasible, which results in the decrease of received power at ID users, and consequently the system SE. Moreover, the performance gain of HUP scheme over the MUB and RUP schemes is evident, suggesting an effective scheme for MISO-NOMA networks under non-linear EH circuit condition.

In Fig. 4(c), we show the effect of the total number of users on the average SE. We set the number of energy users as $K = 12$, the number of ID users as $M = N \in [2, 5]$, and number antennas as $L = 7$. The average SE first increases and achieves its maximum at 18 users ($K = 12, M = N = 3$), then it degrades with M and N. The reason is that the system lacks of the available DoF for leveraging multiuser diversity when the number of ID users is larger than the number of antennas at the BS. Therefore, the system can serve a larger set of users as long as it still maintains the available DoF for transmission. Again, the proposed HUP scheme shows its highest SE performance over the existing ones.

In Fig. 5(a), we show the average EE as a function of the power budget $P_{\rm BS}^{\max}$ with different target rate thresholds $\bar{\rm R}$. As can be observed, the EE of all schemes is very small at the low value of $P_{\rm BS}^{\max}$ because the EE is proportional to the system SE at low value of the $P_{\rm BS}^{\max}$, especially the HUP w/o EB scheme witnesses the worst performance. When $P_{\rm BS}^{\max}$ is increased, the EE of all schemes is also escalated. However, for a sufficiently large $P_{\rm BS}^{\max}$, the system EE is not increase any more due to the effect of large power consumption. The EE of the HUP w/o EB scheme is asymptotic to the HUP one at high region of $P_{\rm BS}^{\max}$, i.e., $P_{\rm BS}^{\max} \geq 40$, because the power budget at the BS is now sufficient to allocate for the information and energy users. Finally, HUP scheme outperforms RUP one which by its turn considerably outperforms MUB one over the whole range of $P_{\rm BS}^{\max}$. The reason is that the HUP scheme using hybrid user pairing approach with optimal pairing factor $[\mathbf{A}]_{mn}$ suppresses the interference from unwanted users in (9), which improves the SE and EE performances. On the other hand, the MUB scheme deploying conventional beamforming results in poor

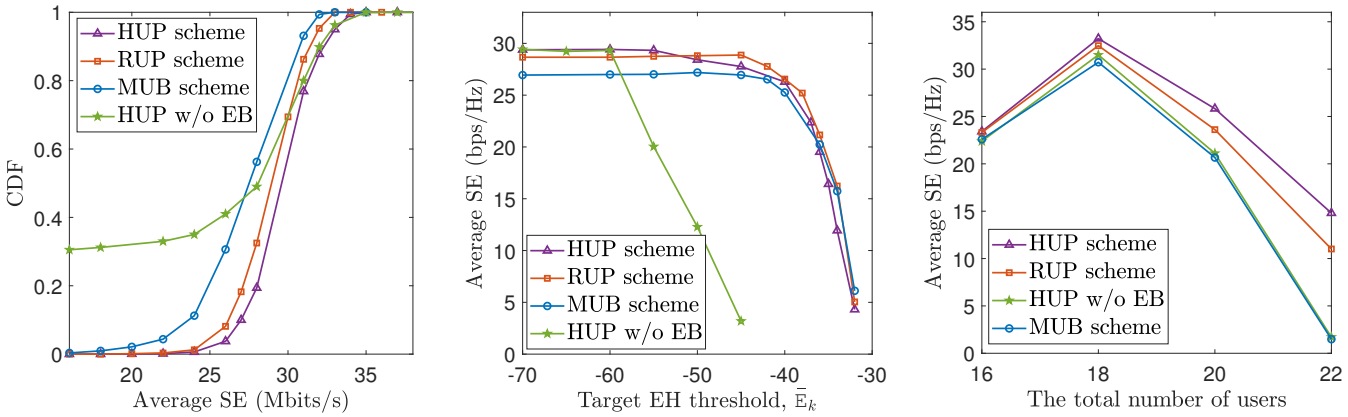

(a) CDF of the system SE (b) Average SE versus $\bar{E}_k$ (c) Average SE versus the number of users

Fig. 4: CDF of the system SE and effects of $\bar{E}_k$ and the number of users on the average SE.

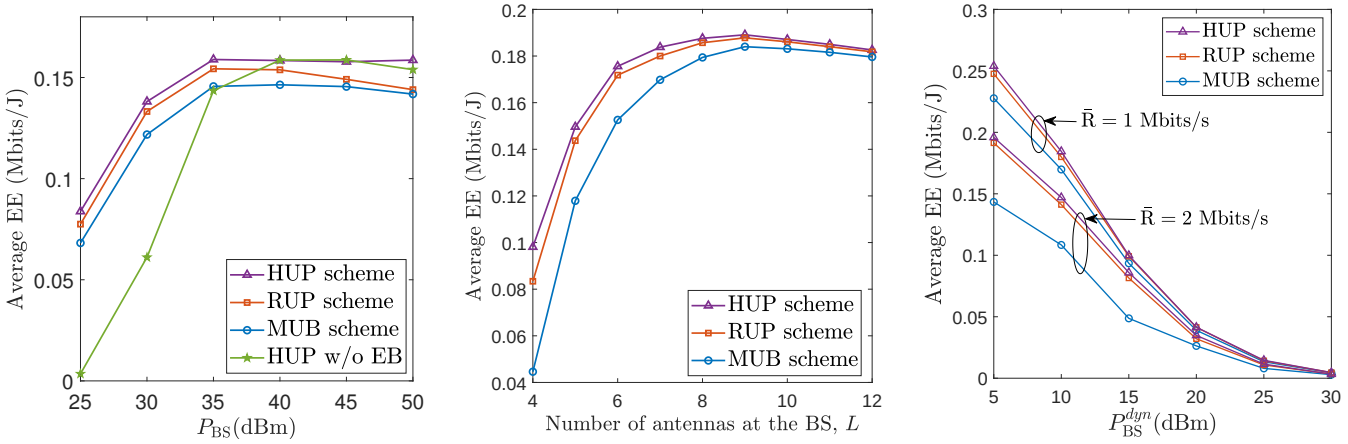

(a) Average EE versus $P_{\mathrm{BS}}^{\max}$ (b) Average EE versus L (c) Average EE versus P_{BS}^{dyn}

Fig. 5: Average EE against P_{BS}^{dyn}, L, and $P_{\mathrm{BS}}^{\max}$.

performance.

Fig. 5(b) depicts the average EE as a function of the number of antennas at the BS L. We can see that the EE of all schemes is first increased and then slightly decreased at a certain value of L. In MISO system, deploying more antennas offers additional DoF, i.e., spatial diversity gain, which by its turn increases the SE, but also consumes more power. When L is small, the increase of SE is higher than that of the total power consumption resulting in the increase of EE. Otherwise, when L is sufficient large, the opposite effect is shown in Fig. 5(b) with the same reason discussed in Fig. 5(c).

We now shift our focus to the effect of dynamic power consumption P_{BS}^{dyn} on average EE for three schemes with different rates $\bar{\mathrm{R}}$ as shown in Fig. 5(c). As expected, the proposed HUP scheme offers a higher EE gain over the RUP and MUB ones, especially at a small value of P_{BS}^{dyn}. The reason is that for small P_{BS}^{dyn}, the power consumption in (15) is dominated by the summation of beamforming power $\mathbf{w}_1, \mathbf{w}_2$ and $\mathbf{V}$, leading to the energy-efficient for all schemes, from which the proposed HUP scheme allocates the power more optimal than the other ones. When P_{BS}^{dyn} is increased, all schemes achieve almost the same energy efficiency and their EE is reduced significantly because the power consumption in (16) is now dominated by the circuit power consumption, resulting in the poor EE performance. A further interesting observation drawn from Fig. 5(c) is that the MUB scheme undergoes considerable degradation in terms of EE compared to HUP scheme when $\bar{\mathrm{R}}$ is increased, which confirms that the proposed HUP scheme can guarantee user-specific QoS at high data rate regime.

Fig. 6(a) reveals effects of priority parameter α on the average EE and EH. We set the target EH threshold $\bar{\mathrm{E}}_k = -55$ dBm, and the minimum rate requirement $\bar{\mathrm{R}}_m = \bar{\mathrm{R}}_m = 1$ bps/Hz. As expected, the HUP scheme always shows its superiority over other ones in terms of EE. As can be observed, three schemes give the same average amount of harvested power because the user pairing method has no effect on EH users. When α is sufficient large, the EE-EH trade-off function

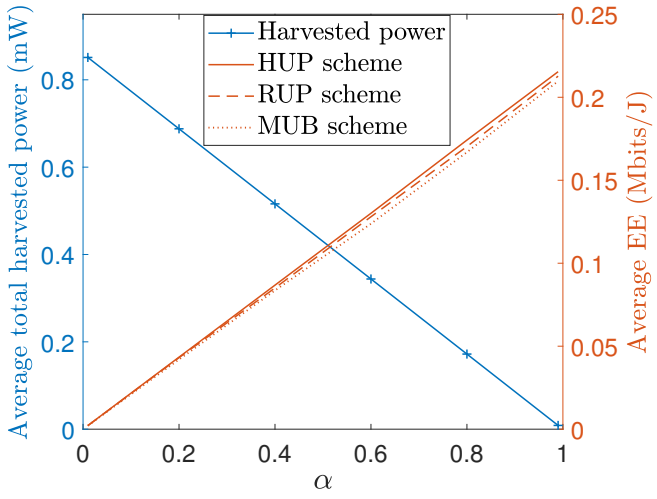

(a) Effects of priority parameter α on the average EH and EE

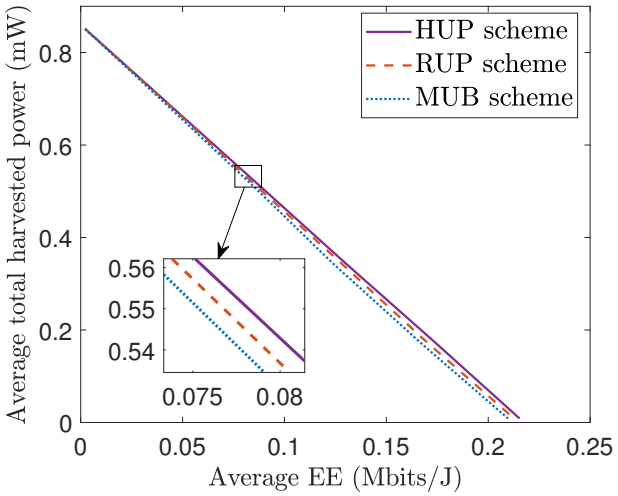

(b) Trade-off between EH and EE with three schemes

Fig. 6: Effects of α on the average EH and EE, and the trade-off EE-EH problem.

reduces to the EEM problem, and the trade-off function (17) reduces to the EH problem when α is relatively small, which are consistent with observations in Remark 2.

In Fig. 6(b), we plot the trade-off between achieved EE and total harvested power, which is accomplished by using the same setup as Fig. 6(a) and sweeping the priority parameter α over interval $[0, 1]$. As can be observed, with respect to α, the average EE is decreased when the average harvested power is increased. The reason is that when α is decreased, the EH problem becomes increasingly dominant in (17), which results in the increase of total harvested power. The opposite effect can be made for EE when α is decreased.

VIII. Conclusions

In this paper, we proposed the hybrid user pairing beamforming in MU-MISO-NOMA systems with SWIPT to improve the spectral and energy efficiencies under a practical non-linear EH circuit model. To improve the SE and EE, we developed the novel HUP scheme to optimally pair two information users, which reduces the number of association users. We then formulated the maximization problems of spectral and energy efficiencies under user-specific QoS requirements, EH constraint and power budget at the BS by jointly optimizing beamformers and pairing matrix. By introducing clever and efficient transformations to approximate the non-convex design problems, we equivalently transformed them into non-convex ones yet with more tractable forms, where binary variables are relaxed to be continuous. The low-complexity IA-framework-based algorithms were proposed for their solutions, which arrive at least local optima with convergence guaranteed. We further considered the general EE-EH trade-off optimization problem which was flexibly switched to the EEM or EH problems depending on the target design of communication systems. Numerical results showed the SE and EE improvements of the proposed HUP scheme over state-of-the-art approaches, i.e., random user pairing and conventional multiuser beamforming schemes.

Appendix A
Proof of Proposition 1

We will show that constraints (20b)-(20e) are hold with equalities at optimum. Denote by $\mathbf{S}^\star \triangleq \{\mathbf{w}^\star, \mathbf{V}^\star, \mathbf{A}^\star, \mathbf{r}^\star, \boldsymbol{\gamma}^\star\}$ the optimal solution of (20). Let us begin with the proof of constraints (20d) and (20e) first by contradiction. Assuming that inequalities of (20d) and (20e) are hold at optimum, i.e., $\ln(1 + 1/\gamma_m^\star) > r_m^\star$ for some m and $\ln(1 + 1/\gamma_n^\star) > r_n^\star$ for some n. There exist $\Delta r_m > 0$ and $\Delta r_n > 0$ that satisfy $\ln(1 + 1/\gamma_m^\star) \geq r_m^\star + \Delta r_m$ and $\ln(1 + 1/\gamma_n^\star) \geq r_n^\star + \Delta r_n$. That is to say $r_m^\star + \Delta r_m$ and $r_n^\star + \Delta r_n$ are also feasible to problem (20), meaning that a strictly larger objective (20a) can be obtained. This contradicts with the assumption that $\mathbf{S}^\star$ is an optimal solution. Thus, it proves that the constraints (20d) and (20e) must hold with equalities at optimum. The similar proof steps can be applied for constraints (20b) and (20c). The optimal solution $(\mathbf{w}^\star, \mathbf{V}^\star, \mathbf{A}^\star)$ of (19) can be obtained easily from the optimal solution set $\mathbf{S}^\star$ of (20), and then they share the same optimal objective value.

Appendix B
Proof of Proposition 2

We now provide a sketch of the proof to verify the convergence of Algorithm 1, and that of Algorithms 2 and 3 follows immediately. Let us denote by $\bar{\mathcal{R}}_\sum(\mathbf{S}_{\texttt{SEM}})$ and $\bar{\mathcal{R}}_\sum^{(\kappa)}(\mathbf{S}_{\texttt{SEM}})$ the objectives of (20) and (39), respectively. Due to the use of inner convex approximations, it is true that

$$\bar{\mathcal{R}}_\sum(\mathbf{S}_{\texttt{SEM}}) \geq \bar{\mathcal{R}}_\sum^{(\kappa)}(\mathbf{S}_{\texttt{SEM}}), \tag{63}$$

and

$$\bar{\mathcal{R}}_\sum(\mathbf{S}_{\texttt{SEM}}^{(\kappa)}) = \bar{\mathcal{R}}_\sum^{(\kappa)}(\mathbf{S}_{\texttt{SEM}}^{(\kappa)}). \tag{64}$$

Recalling that approximate functions presented in Sections III satisfy property A given in [42]. That is to say, the optimal solution obtained at iteration κ is also feasible to the convex program (39) at iteration $(\kappa+1)$ for the SEM problem. As a result, we have

$$\begin{aligned}\bar{\mathcal{R}}_{\sum}(\mathbf{S}_{\mathtt{SEM}}^{(\kappa+1)}) &= \bar{\mathcal{R}}_{\sum}^{(\kappa+1)}(\mathbf{S}_{\mathtt{SEM}}^{(\kappa+1)}) \geq \bar{\mathcal{R}}_{\sum}^{(\kappa)}(\mathbf{S}_{\mathtt{SEM}}^{(\kappa+1)}) \\ &\geq \bar{\mathcal{R}}_{\sum}^{(\kappa)}(\mathbf{S}_{\mathtt{SEM}}^{(\kappa)}) = \bar{\mathcal{R}}_{\sum}(\mathbf{S}_{\mathtt{SEM}}^{(\kappa)}). \end{aligned} \tag{65}$$

This shows that $\mathbf{S}_{\mathtt{SEM}}^{(\kappa+1)}$ is a better solution for (20) than $\mathbf{S}_{\mathtt{SEM}}^{(\kappa)}$. It also holds true for (19) due to Proposition 1. Since the sequence $\{\mathbf{S}_{\mathtt{SEM}}^{(\kappa)}\}$ is bounded, there exists a stationary point $\bar{\mathbf{S}}_{\mathtt{SEM}}$ so that:

$$\lim_{\kappa\to+\infty} \bar{\mathcal{R}}_{\sum}(\mathbf{S}_{\mathtt{SEM}}^{(\kappa)}) = \bar{\mathcal{R}}_{\sum}(\bar{\mathbf{S}}_{\mathtt{SEM}}). \tag{66}$$

By [34, Theorem 1], the stationary point $\bar{\mathbf{S}}_{\mathtt{SEM}}$ of the sequence $\{\mathbf{S}_{\mathtt{SEM}}^{(\kappa)}\}$ is a KKT point. As a result, Algorithm 1 generates a non-decreasing sequence of objectives, i.e., $\bar{\mathcal{R}}_{\sum}^{(\kappa+1)} \geq \bar{\mathcal{R}}_{\sum}^{(\kappa)}$, which is upper bounded due to the power constraint. Thus, Algorithm 1 is probably convergent.

REFERENCES

[1] Z. Ding, Y. Liu, J. Choi, Q. Sun, M. Elkashlan, I. Chih-Lin, and H. V. Poor, "Application of non-orthogonal multiple access in LTE and 5G networks," *IEEE Commun. Mag.*, vol. 55, no. 2, pp. 185–191, Feb. 2017.

[2] L. Dai, B. Wang, Z. Ding, Z. Wang, S. Chen, and L. Hanzo, "A survey of non-orthogonal multiple access for 5G," *IEEE Commun. Surveys Tuts.*, vol. 20, no. 3, pp. 2294–2323, 3rd Quart. 2018.

[3] Z. Ding, F. Adachi, and H. V. Poor, "The application of MIMO to non-orthogonal multiple access," *IEEE Trans. Wireless Commun.*, vol. 15, no. 1, pp. 537–552, 2016.

[4] H. V. Nguyen, V.-D. Nguyen, O. A. Dobre, D. N. Nguyen, E. Dutkiewicz, and O.-S. Shin, "Joint power control and user association for NOMA-based full-duplex systems," *IEEE Trans. Commun.*, vol. 67, no. 11, pp. 8037–8055, Nov. 2019.

[5] V.-D. Nguyen, H. D. Tuan, T. Q. Duong, H. V. Poor, and O.-S. Shin, "Precoder design for signal superposition in MIMO-NOMA multicell networks," *IEEE J. Sel. Areas Commun.*, vol. 35, no. 12, pp. 2681–2695, Dec. 2017.

[6] M. S. Ali, H. Tabassum, and E. Hossain, "Dynamic user clustering and power allocation for uplink and downlink non-orthogonal multiple access (NOMA) systems," *IEEE Access*, vol. 4, pp. 6325–6343, Aug. 2016.

[7] Z. Ding, P. Fan, and H. V. Poor, "Impact of user pairing on 5G nonorthogonal multiple-access downlink transmissions," *IEEE Trans. Veh. Tech.*, vol. 65, no. 8, pp. 6010–6023, Aug. 2016.

[8] T. D. P. Perera, D. N. K. Jayakody, S. K. Sharma, S. Chatzinotas, and J. Li, "Simultaneous wireless information and power transfer (SWIPT): Recent advances and future challenges," *IEEE Commun. Surveys Tuts.*, vol. 20, no. 1, pp. 264–302, 1st Quart. 2018.

[9] E. Boshkovska, D. W. K. Ng, N. Zlatanov, and R. Schober, "Practical non-linear energy harvesting model and resource allocation for SWIPT systems," *IEEE Commun. Lett.*, vol. 19, no. 12, pp. 2082–2085, Dec. 2015.

[10] J. Guo and X. Zhu, "An improved analytical model for RF-DC conversion efficiency in microwave rectifiers," in *IEEE MTT-S Int. Microw. Symp. Dig.* IEEE, Jun. 2012, pp. 1–3.

[11] L. Zhu, J. Zhang, Z. Xiao, X. Cao, and D. O. Wu, "Optimal user pairing for downlink non-orthogonal multiple access (NOMA)," *IEEE Wirel. Commun. Le.*, pp. 1–4, Jul. 2018.

[12] W. Liang, Z. Ding, Y. Li, and L. Song, "User pairing for downlink non-orthogonal multiple access networks using matching algorithm," *IEEE Trans. Commun.*, vol. 65, no. 12, pp. 5319–5332, Dec. 2017.

[13] Z. Ding, M. Peng, and H. V. Poor, "Cooperative non-orthogonal multiple access in 5G systems," *IEEE Commun. Lett.*, vol. 19, no. 8, pp. 1462–1465, Aug. 2015.

[14] L. Zhu, J. Zhang, Z. Xiao, X. Cao, D. O. Wu, and X.-G. Xia, "Millimeter-wave NOMA with user grouping, power allocation and hybrid beamforming," *IEEE Trans. Wireless Commun.*, vol. 18, no. 11, pp. 5065–5079, Nov. 2019.

[15] L. Dai, B. Wang, M. Peng, and S. Chen, "Hybrid precoding-based millimeter-wave massive MIMO-NOMA with simultaneous wireless information and power transfer," *IEEE Journal on Selected Areas in Communications*, vol. 37, no. 1, pp. 131–141, Jan. 2019.

[16] X. Chen, F.-K. Gong, G. Li, H. Zhang, and P. Song, "User pairing and pair scheduling in massive MIMO-NOMA systems," *IEEE Commun. Lett.*, vol. 22, no. 4, pp. 788–791, Apr. 2017.

[17] Y. Liu, M. Elkashlan, Z. Ding, and G. K. Karagiannidis, "Fairness of user clustering in MIMO non-orthogonal multiple access systems," *IEEE Commun. Lett.*, vol. 20, no. 7, pp. 1465–1468, 2016.

[18] B. Su, Q. Ni, and W. Yu, "Robust transmit beamforming for SWIPT-enabled cooperative NOMA with channel uncertainties," *IEEE Trans. Commun.*, vol. 67, no. 6, pp. 4381–4392, Jun. 2019.

[19] X. Zhang, Y. Wang, F. Zhou, N. Al-Dhahir, and X. Deng, "Robust resource allocation for MISO cognitive radio networks under two practical non-linear energy harvesting models," *IEEE Commun. Lett.*, vol. 22, no. 9, pp. 1874–1877, Sept. 2018.

[20] Z. Sheng, H. D. Tuan, T. Q. Duong, and H. V. Poor, "Beamforming optimization for physical layer security in MISO wireless networks," *IEEE Trans. Signal Process.*, vol. 66, no. 14, pp. 3710–3723, Jul. 2018.

[21] Y. Xu, C. Shen, Z. Ding, X. Sun, S. Yan, G. Zhu, and Z. Zhong, "Joint beamforming and power-splitting control in downlink cooperative SWIPT NOMA systems," *IEEE Trans. Signal Process.*, vol. 65, no. 18, pp. 4874–4886, Sept. 2017.

[22] O. Tervo, A. Tölli, M. Juntti, and L. Tran, "Energy-efficient beam coordination strategies with rate-dependent processing power," *IEEE Trans. Signal Process.*, vol. 65, no. 22, pp. 6097–6112, Nov. 2017.

[23] O. Tervo, L.-N. Tran, H. Pennanen, S. Chatzinotas, B. Ottersten, and M. Juntti, "Energy-efficient multicell multigroup multicasting with joint beamforming and antenna selection," *IEEE Trans. Signal Process.*, vol. 66, no. 18, pp. 4904–4919, Sept. 2018.

[24] O. Amin, E. Bedeer, M. H. Ahmed, and O. A. Dobre, "Energy efficiency–spectral efficiency tradeoff: A multiobjective optimization approach," *IEEE Trans. Veh. Tech.*, vol. 65, no. 4, pp. 1975–1981, 2015.

[25] J. Tang, D. K. So, E. Alsusa, K. A. Hamdi, and A. Shojaeifard, "On the energy efficiency–spectral efficiency tradeoff in MIMO-OFDMA broadcast channels," *IEEE Trans. Veh. Tech.*, vol. 65, no. 7, pp. 5185–5199, Jul. 2015.

[26] Q.-D. Vu, L.-N. Tran, R. Farrell, and E.-K. Hong, "An efficiency maximization design for SWIPT," *IEEE Signal Process. Lett.*, vol. 22, no. 12, pp. 2189–2193, 2015.

[27] Z. Chang, L. Lei, H. Zhang, T. Ristaniemi, S. Chatzinotas, B. Ottersten, and Z. Han, "Energy-efficient and secure resource allocation for multiple-antenna NOMA with wireless power transfer," *IEEE Trans. Green Commun. Netw.*, vol. 2, no. 4, pp. 1059–1071, Jul. 2018.

[28] V.-D. Nguyen and O.-S. Shin, "An efficient design for NOMA-assisted MISO-SWIPT systems with AC computing," *IEEE Access*, vol. 7, pp. 97 094–97 105, Jul. 2019.

[29] S. Mao, S. Leng, J. Hu, and K. Yang, "Power minimization resource allocation for underlay MISO-NOMA SWIPT systems," *IEEE Access*, vol. 7, pp. 17 247–17 255, Jan. 2019.

[30] Y. Yuan, P. Xu, Z. Yang, Z. Ding, and Q. Chen, "Joint robust beamforming and power-splitting ratio design in SWIPT-based cooperative NOMA systems with CSI uncertainty," *IEEE Trans. Veh. Tech.*, vol. 68, no. 3, pp. 2386–2400, Mar. 2019.

[31] Q. Qi, X. Chen, and D. W. K. Ng, "Robust beamforming for NOMA-based cellular massive IoT with SWIPT," *IEEE Trans. Signal Process.*, vol. 68, p. 211, Dec. 2020.

[32] O. Tervo, L.-N. Tran, and M. Juntti, "Optimal energy-efficient transmit beamforming for multi-user MISO downlink," *IEEE Trans. Signal Process.*, vol. 63, no. 20, pp. 5574–5588, 2015.

[33] M. F. Hanif, Z. Ding, T. Ratnarajah, and G. K. Karagiannidis, "A minorization-maximization method for optimizing sum rate in the downlink of non-orthogonal multiple access systems." *IEEE Trans. Signal Process.*, vol. 64, no. 1, pp. 76–88, 2016.

[34] B. R. Marks and G. P. Wright, "A general inner approximation algorithm for nonconvex mathematical programs," *Operations research*, vol. 26, no. 4, pp. 681–683, 1978.

[35] Q. Shi, L. Liu, W. Xu, and R. Zhang, "Joint transmit beamforming and receive power splitting for MISO SWIPT systems," *IEEE Trans. Wireless Commun.*, vol. 13, no. 6, pp. 3269–3280, 2014.

[36] Z. Ding, R. Schober, and H. V. Poor, "A general MIMO framework for NOMA downlink and uplink transmission based on signal alignment," *IEEE Trans. Wireless Commun.*, vol. 15, no. 6, pp. 4438–4454, Jun. 2016.

[37] S. Timotheou, I. Krikidis, G. Zheng, and B. Ottersten, "Beamforming for MISO interference channels with QoS and RF energy transfer," *IEEE Trans. Wireless Commun.*, vol. 13, no. 5, pp. 2646–2658, 2014.

[38] D. Nguyen, L.-N. Tran, P. Pirinen, and M. Latva-aho, "On the spectral efficiency of full-duplex small cell wireless systems," *IEEE Trans. Wireless Commun.*, vol. 13, no. 9, pp. 4896–4910, 2014.
[39] K. Wang, Y. Liu, Z. Ding, A. Nallanathan, and M. Peng, "User association and power allocation for multi-cell non-orthogonal multiple access networks," *IEEE Trans. Wireless Commun.*, Aug. 2019.
[40] O. Arnold, F. Richter, G. Fettweis, and O. Blume, "Power consumption modeling of different base station types in heterogeneous cellular networks," in *2010 Future Network Mobile Summit*, vol. 2010. IEEE, Jun. 2010, pp. 1–8.
[41] R. T. Marler and J. S. Arora, "Survey of multi-objective optimization methods for engineering," *Struct. Multidiscip. Optim.*, vol. 26, no. 6, pp. 369–395, 2004.
[42] A. Beck, A. Ben-Tal, and L. Tetruashvili, "A sequential parametric convex approximation method with applications to nonconvex truss topology design problems," *J. Global Optim.*, vol. 47, no. 1, pp. 29–51, May 2010.
[43] V.-D. Nguyen, T. Q. Duong, H. D. Tuan, O.-S. Shin, and H. V. Poor, "Spectral and energy efficiencies in full-duplex wireless information and power transfer," *IEEE Trans. Commun.*, vol. 65, no. 5, pp. 2220–2233, 2017.
[44] V. Nguyen, H. V. Nguyen, O. A. Dobre, and O. Shin, "A new design paradigm for secure full-duplex multiuser systems," *IEEE J. Sel. Areas Commun.*, vol. 36, no. 7, pp. 1480–1498, Jul. 2018.
[45] Z. Chen, Z. Ding, and X. Dai, "Beamforming for combating inter-cluster and intra-cluster interference in hybrid NOMA systems," *IEEE Access*, vol. 4, pp. 4452–4463, 2016.
[46] K.-C. Toh, M. J. Todd, and R. H. Tütüncü, "SDPT3—a MATLAB software package for semidefinite programming, version 1.3," *Optim. Methods Softw.*, vol. 11, no. 1-4, pp. 545–581, Jan. 1999.
[47] J. Löfberg, "YALMIP: A toolbox for modeling and optimization in MATLAB," in *Proc. IEEE Int. Symp. Comput. Aided Control Syst. Design*, vol. 3. Taipei, Taiwan, Sept. 2004.

Toan-Van Nguyen (S'19) received the B.S. degree in electronics and telecommunications engineering and the M.S. degree in electronics engineering from Ho Chi Minh City University of Technology and Education, Vietnam, in 2011 and 2014, respectively. He is currently pursuing the Ph.D. degree with the Department of Electronics and Computer Engineering in Graduate School, Hongik University, Republic of Korea. His current research activity is focused on the mathematical modeling of 5G networks and machine learning for wireless communications.

Van-Dinh Nguyen (S'14-M'19) received the B.E. degree in electrical engineering from Ho Chi Minh City University of Technology, Vietnam, in 2012 and the M.E. and Ph.D. degrees in electronic engineering from Soongsil University, Seoul, South Korea, in 2015 and 2018, respectively. He is currently a Research Associate with the Interdisciplinary Centre for Security, Reliability and Trust (SnT), University of Luxembourg. He was a Postdoc Researcher and a Lecturer with Soongsil University, a Postdoctoral Visiting Scholar with University of Technology Sydney, AUS (July-August 2018) and a Ph.D. Visiting Scholar with Queen's University Belfast, U.K. (June-July 2015 and August 2016). His current research activity is focused on the mathematical modeling of 5G cellular networks and machine learning for wireless communications.

Dr. Nguyen received several best conference paper awards, the Exemplary Editor Award of IEEE COMMUNICATIONS LETTERS 2019, IEEE TRANSACTION ON COMMUNICATIONS Exemplary Reviewer 2018 and IEEE GLOBECOM Student Travel Grant Award 2017. He has authored or co-authored in some 40 papers published in international journals and conference proceedings. He has served as a reviewer for many top-tier international journals on wireless communications, and has also been a Technical Programme Committee Member for several flag-ship international conferences in the related fields. He is an Editor for the IEEE OPEN JOURNAL OF THE COMMUNICATIONS SOCIETY and IEEE COMMUNICATIONS LETTERS.

Daniel Benevides da Costa (S'04-M'08-SM'14) was born in Fortaleza, Ceará, Brazil, in 1981. He received the B.Sc. degree in Telecommunications from the Military Institute of Engineering (IME), Rio de Janeiro, Brazil, in 2003, and the M.Sc. and Ph.D. degrees in Electrical Engineering, Area: Telecommunications, from the University of Campinas, SP, Brazil, in 2006 and 2008, respectively. His Ph.D thesis was awarded the Best Ph.D. Thesis in Electrical Engineering by the Brazilian Ministry of Education (CAPES) at the 2009 CAPES Thesis Contest. From 2008 to 2009, he was a Postdoctoral Research Fellow with INRS-EMT, University of Quebec, Montreal, QC, Canada. Since 2010, he has been with the Federal University of Ceará, where he is currently an Associate Professor.

Prof. da Costa is currently Executive Editor of the IEEE COMMUNICATIONS LETTERS and Area Editor of IEEE OPEN JOURNAL OF THE COMMUNICATION SOCIETY – Area: Green, Cognitive, and Intelligent Communications and Networks. He is also Editor of the IEEE COMMUNICATIONS SURVEYS AND TUTORIALS, IEEE TRANSACTIONS ON COMMUNICATIONS, IEEE TRANSACTIONS ON VEHICULAR TECHNOLOGY, and IEEE TRANSACTIONS ON COGNITIVE COMMUNICATIONS AND NETWORKING. He has also served as Associate Technical Editor of the IEEE COMMUNICATIONS MAGAZINE. From 2012 to 2017 and from March 2019 to August 2019, he was Editor and Senior Editor, respectively, of the IEEE COMMUNICATIONS LETTERS. He has served as Lead Guest Editor and Guest Editor of several Journal Special Issues. He has been involved on the Organizing Committee of several conferences. He is currently the Latin American Chapters Coordinator of the IEEE Vehicular Technology Society. Also, he acts as a Scientific Consultant of the National Council of Scientific and Technological Development (CNPq), Brazil, and he is a Productivity Research Fellow of CNPq. From 2012 to 2017, he was Member of the Advisory Board of the Ceará Council of Scientific and Technological Development (FUNCAP), Area: Telecommunications. Currently, he is Vice-Chair of Americas of the IEEE Technical Committee of Cognitive Networks (TCCN), Director of the TCCN Newsletter, and Chair of the Special Interest Group on "Energy-Harvesting Cognitive Radio Networks" in IEEE TCCN.

Prof. da Costa is the recipient of four conference paper awards. He received the Exemplary Reviewer Certificate of the IEEE WIRELESS COMMUNICATIONS LETTERS in 2013 and 2019, the Exemplary Reviewer Certificate of the IEEE COMMUNICATIONS LETTERS in 2016, 2017, and 2019, the Certificate of Appreciation of Top Associate Editor for outstanding contributions to IEEE TRANSACTIONS ON VEHICULAR TECHNOLOGY in 2013, 2015 and 2016, the Exemplary Editor Award of IEEE COMMUNICATIONS LETTERS in 2016, and the Outstanding Editor Award of IEEE ACCESS in 2017, and the Certificate of Appreciation for notable services and contributions to IEEE ACCESS in 2018 and 2019. He is a Distinguished Lecturer of the IEEE Vehicular Technology Society. He is a Senior Member of IEEE, Member of IEEE Communications Society and IEEE Vehicular Technology Society.

Beongku An received the B.S. degree in electronic engineering from Kyungpook National University, Republic of Korea, in 1988, the M.S. degree in electrical engineering from the New York University (Polytechnic), NY, USA, in 1996 and Ph.D. degree from New Jersey Institute of Technology (NJIT), NJ, USA, in 2002, respectively. After graduation, he joined the Faculty of the Department of Software and Communications Engineering, Hongik University, Republic of Korea, where he is currently a Professor. From 1989 to 1993, he was a senior researcher in RIST, Pohang, Republic of Korea. He also was lecturer and RA in NJIT from 1997 to 2002. He was a president of IEIE Computer Society (The Institute of Electronics and Information Engineers, Computer Society) in 2012. From 2013, he also works as a General Chair in the International Conference, ICGHIT (International Conference on Green and Human Information Technology). His current research interests include mobile wireless networks and communications such as ad-hoc networks, sensor networks, wireless cognitive radio networks, cellular networks. In particular, he is interested in cooperative communication, multicast routing, QoS routing, energy harvesting, physical layer security, M2M/D2D, IoT, visible light communication (VLC), cross-layer technology, 5G/Beyond 5G, NOMA, SWIPT, Machine Learning & Block Chain, mobile cloud computing. Professor An was listed in Marquis Who's Who in Science and Engineering, and Marquis Who's Who in the World, respectively.